공학석사 학위논문

Linear and Nonlinear Micromechanics Model for CNT Nanocomposites with Stochastic Simulation

확률적 카본나노튜브 나노복합재료를 위한 선형 & 비선형 미소역학 모델

2019 년 8 월

서울대학교 대학원

기계항공공학부

주비연

Linear and Nonlinear Micromechanics Model for CNT Nanocomposites with Stochastic Simulation

확률적 카본나노튜브 나노복합재료를 위한 선형 &
비선형 미소역학 모델

지도 교수 윤 군 진

이 논문을 공학석사 학위논문으로 제출함

2019 년 8 월

서울대학교 대학원

기계항공공학부

주 비 연

주비연의 공학석사 학위논문을 인준함

2019 년 8 월

위 원 장 김 지 환 (인)

부위원장 윤 군 진 (인)

위 원 신 상 준 (인)

Abstract

Linear and Nonlinear Micromechanics Model for CNT Nanocomposites with Stochastic Simulation

Feiyan Zhu

Department of Mechanical and Aerospace Engineering

The Graduate School

Seoul National University

Owing to excellent mechanical, electrical and chemical properties, Carbon Nanotube (CNT) has been researched as promising nanofiller for various applications such as structural materials, stealth materials, sensors, capacitors, electrical devices, etc. Researches on CNT nanocomposites have experienced significant advances especially in the synthesis and manufacturing technologies. However, in spite of such advances in material science and engineering, design, modelling

and analysis of the CNT nanocomposites are relatively less matured because of complex nature of morphology, non-uniform dispersion, and involvement of complex multiphysics. Moreover, modeling of the nanoscale CNT fillers and upscaling to macro experimental scale inherently require multiscale approach. In order to bridge nanoscale feature with predictions at the macroscale, micromechanics and homogenization is crucially important core technology.

In this thesis, a new approach to nonlinear micromechanics models for CNT nanocomposites was proposed, which will be a framework for stochastic multiscale modeling and analysis of general nanocomposites. Specifically, a stochastic modeling framework was proposed that can model spatially random design variables of nano-sized fillers in the three-dimensional space. This stochastic modeling technique was applied to statistical orientations of nano-fillers. Then, this thesis focuses on Mori-Tanaka micromechanics model, which is well-accepted homogenization method. In this thesis, ductile damage plasticity of polymer matrix and interface damage between matrix and CNT nanofillers were modelled within the incremental and iterative Mori-Tanaka micromechanics modeling framework. To

simulate interfacial damage, linear spring model (LSM) was combined with Mori-Tanaka method. Also, effects of CNT fiber orientation on effective stiffness of the nanocomposites were studied. Plastic properties are provided by using J2 flow rule and Lemaitre-Chaboche damage modeling method. Nonlinear hardening function was used in the model. Numerical analyses considered volume fraction, aspect ratio, interfacial damage and ductile damage. It was shown that the elasto-plastic properties are greatly influenced by damage, both ductile and interfacial, and other composites material properties.

Keywords : Stochastic simulation, Ductile damage, Mori-Tanaka method, Interfacial damage, CNT nanocomposites

Student Number : 2017-21362

Table of contents

List of figures

List of tables

1. Introduction

1.1. Background and motivation

Carbon nanotubes (CNT), as one of most popular materials in 21st century, own great mechanical properties including a Young's modulus of 1TPa, tensile strength 20 times that of high-strength steel alloys, and thermal conductivity of almost double that of pure diamond [1]. Since CNTs were first discovered in 1991 by Iijima [2], many researchers have conducted plenty of studies on CNT nano-fillers from different perspectives [3-7]. CNT is an excellent reinforcing filler for polymeric matrix composite whose properties are influenced by various factors, for instance, waviness, dispersion, fiber orientation, bonding conditions and interphase materials between the CNT fibers and matrix. All these factors have great influences on mechanical and electrical properties of the CNT-reinforced polymeric nanocomposite materials.

With various models, studies were proposed to simulate the effective properties of CNT nanocomposites [8, 9]. The effects of

inner fiber and matrix properties, waviness, interfacial debonding and dispersions of CNTs render disputes on comparisons between experimental data and theoretical predictions. Therefore, modeling efforts have focused on those geometric features of CNTs which are complicated with various factors. For instance, Hammerand et al. reported that the effects of the interphase regions on the effective properties are more significant than the clustering effects [10]. Fisher et al. [11] reported that the waviness and orientations can also reduce the effective stiffness. Then, following the work by Fisher et al., Bradshaw et al. counted for waviness effects of CNTs and proposed a prediction method of aligned or randomly oriented composite properties, which is linked with dispersion of fibers in CNT nanocomposites via finite elements and Mori-Tanaka micromechanics theory [12]. Shao et al. recognized a significant influence of the waviness and interfacial debonding on the reinforcement efficiency of CNTs [14]. Anumandla et al. proposed a closed-form effective stiffness model by incorporating waviness and random orientation of the CNTs in matrix materials [15]. Shockrieh et al. provided review of three existing modeling approaches of CNT

nanocomposite materials which are atomistic, analytical continuum and numerical continuum approaches [10]. Shockrieh et al. stated advantages, limitations and drawbacks of each of the models. Odegard et al. proposed a constitutive modeling approach for the randomly oriented and aligned CNT nanocomposites [17].

In general, large variations in the experimental observations could be dealt with through stochastic modeling. According to literature surveys, there are few studies on the stochastic modeling of CNT nanocomposites.

Probabilistic approach has been adopted on electrical properties [18] and molecular dynamics [19] of the CNT nanocomposites at the microscale. However, no model for stochastically-aligned wavy CNT exists which will be introduced in this thesis.

Not only linear damage models for CNT nanocomposites, which simulate elastic conditions, but also nonlinear plasticity models attract more attentions. Oller first presented a plastic damage model for concrete structures with finite element method in 1990 [78]. Sun and Chen [79] discovered a simple flow rule to discuss nonlinear behavior of fiber composites in 1989. Based on Sun and Chen's work,

Kyriakides did research on compressive failure [80] and Schapery extended to visco-elasto-plasticity of composites on thermal dynamics [81]. And then in 2000, Mirmiran provided a finite element model for fiber composites [82] and an improved nonlinear model with interphase was presented [83]. In the line of former researches, we build a model for CNT nanocomposites with interfacial damage and damage plasticity to simulate the effective nonlinear micromechanical behavior.

1.2. Objectives and thesis overview

This thesis presents a new probabilistic approach to model the random distributions of the elastic properties within 3D microscale continuum RVE while taking into account the spatial randomness of the CNTs' waviness, interfacial stiffness and dispersion. The novelty of this thesis includes a direction-sensitive 3D Karhunen-Loève expansion (KLE) method, modelling stochastically aligned CNT-reinforced polymer matrix, and new investigations on how statistical parameters at the nanoscale affect the microscale RVE size. Also, a modified Mori-Tanaka simulation will be proposed to implement in

the wavy CNT nanocomposites model with interfacial damage. Then, we introduce linear and nonlinear Mori–Tanaka model to deal with elastic and plastic range of CNT nanocomposites. Section 2 will describe three main micromechanics models, which are classic micromechanics model, computational model and Mori–Tanaka homogenization model. All these three models are universally in the researches. Then, in Section 3, we will introduce the direction–sensitive KLE method used to model the random 3D fields. Section 4 provides the improved linear Mori–Tanaka model and Section 5 focuses on elasto–plastic properties with nonlinear MT model and overview of the proposed modeling framework. Numerical results are presented in Section 6 which are divided into several parts to show the simulation in Section 3–5. In Section 7, we will discuss the conclusions and what we can extend based on current work in the future.

2. Micro mechanics model for CNT nanocomposites

2.1. Classic micromechanics models

CNT nanocomposite is a typical fiber inclusion composite which can be simulated by using most homogenization method. For composites. Chamis provided a simplified micromechanics models (SMM) with rule of mixture (ROM) by using material properties of the inclusion and matrix. Various composites materials and boundary conditions [21−25] are applied with rule of mixture. Also, this universally used micromechanics model to predict the elastic properties for fiber composites is Halpin and Tsai's model. They first proposed the Halpin−Tsai's Equation [26] in 1976 which is based on Hill's self−consistent micromechanics method. This equation was quickly introduced in the CNT composites model [27, 28].

Then, to use simple relations among fiber size and volume fraction, Hopkins and Chamis [29] developed a refined model for shear and transverse properties and have been proposed in many fiber like inclusion composites [30, 31].

2.2. Computational micromechanics models

The finite element model is most widely used computational micromechanics model since it can deal with complicated fiber packing with accuracy. Caruso and Chamis [32] developed a single-cell finite element model in 1986. Then, Finegan, and Gibson provided examples of 2D and 3D finite element quarter domain models [33]. After that, more and more researchers adopted finite element models in CNT nanocomposites simulation at the microscale [34-36].

2.3. Mori-Tanaka micromechanics models

Mori-Tanaka (MT) method is a universally used and classical method that was proposed in 1981 to predict the effective stiffness of various composite materials [37-39]. Numerous researches on its extension and application have been conducted. For example, Mori-Takana approach has been extended for incremental formulation of thermo-elasto-plastic constitutive law [40-45], and interface debonding [46, 47] model is also considered. Homogenization of elastic-viscoplastic heterogeneous materials [35], and combination with self-consistent approach [49], and prediction of the effective

thermal conductivity [50, 51], etc. were also studied by researchers. MT model has also been applied for CNT nanocomposites [52–54], functionally graded materials [55, 56], porous materials [57], etc. In the meanwhile, Eshelby tensor in the MT method was introduced to describe reinforcing inclusions with interphase weakness since the slightly weakened interfaces are commonly observed [58]. Following the Qu's approach, the linear spring model was adopted for interface damage between CNT and polymer matrix by many researchers [59–62]. Recently, Ryu et al. corrected mathematical and typographical errors in an interfacial damage tensor denoted by Q (i.e. specifically Q_{1122}, Q_{1111}, and Q_{2222}) in previous studies [63]. Tsai, et al. systematically investigated stochastic effects of CNT inclusions waviness and its distribution to the effective stiffness [64]. Shao et al. studied the waviness of CNT and interface debonding behavior, which are the two key factors that influence reinforcing efficiency [14].

3. Spatial randomness modeling for CNT morphology

CNT nanocomposites is one of most popular composites applied in wide fields, for instance, aerospace, electronic and mechanical areas, because its significant mechanical and electrical performance. However, the structure of CNT nanocomposites is complicated, so we cannot do the simulation simply with single fiber and matrix base. Shape variety cannot be ignored. The variety covers not only waviness, volume fraction, which are material properties, but also include fiber orientation and correlation length.

In this section, we will provide a novel method to develop 3D random fields while, in presented documents, it is commonly to use 2D random fields. 3D randomness provides convenience in simulating spatial models and we can not only apply the random fields in examples we presented in the thesis, but also in other stochastic simulations for future research.

3.1. Modeling of random fields

To satisfy the randomness of composites material, random field generator, 3D Karhunen−Loeve Expansion method, is adopted in this thesis. The main idea of this method is to discrete the continuous field into a deterministic part and a discontinuous stochastic part which can be described by eigenvalues and eigenvectors.

The three−dimensional KLE decomposes a spatial random field $H(x', y', z', \omega)$ to a deterministic and a stochastic part with series of expansion as follows to model spatially distributed materials

$$H(x', y', z', \omega) = \langle H \rangle + \sum_{i=1}^{m} \sqrt{\lambda_i} \phi_i(x', y', z')[\xi_i(\omega)] \qquad (1)$$

Where $\langle H \rangle$ the mean value; ω is the primitive randomness; ξ_i is the normal variable; λ_i and ϕ_i are the eigenvalue and eigenfunction of the analytical covariance kernel, respectively; m is the truncation order of KLE; and x', y' and z' are coordinate values in the prime coordinate system. The solutions of the following Fredholm integral equation in Equation (2) are λ_i and ϕ_i.

$$\int_{\Omega_{2e}}^{1} C(\vec{X}_1, \vec{X}_2)\, \phi_k(\vec{X}_2) dV_{2e} = \lambda_k \phi_k(\overrightarrow{X_1}) \qquad (2)$$

Where $\overrightarrow{X_1}(x_1', y_1', z_1')$ and $\overrightarrow{X_2}(x_2', y_2', z_2')$ are two randomly selected points in the prime coordinate system. We assumed an exponential form of the covariance function $C(\overrightarrow{X_1}, \overrightarrow{X_2})$ as

$$C(\overrightarrow{X_1}, \overrightarrow{X_2}) = \sigma^2 exp\left(-\frac{|x_1' - x_2'|}{L_x} - \frac{|y_1' - y_2'|}{L_y} - \frac{|z_1' - z_2'|}{L_z}\right) \qquad (3)$$

where L_i is the correlation length in the i^{th} direction; and σ is the standard deviation. The correlation length is a statistical parameter that measures spatial correlation of random fields. For example, a large correlation length means high correlation of the random field between two points, which physically results in smooth change of the random field between the two points. On the contrary, a small correlation length mean low correlation of the random field between the two points, resulting in high fluctuation of the random field. The prime coordinate $(x' - y' - z')$ is rotated to a non−prime coordinate system $(x - y - z)$ by the rotational transformation.

$$\{x'\} = [R][x] = \begin{bmatrix} \frac{\partial x'}{\partial x} & \frac{\partial x'}{\partial y} & \frac{\partial x'}{\partial z} \\ \frac{\partial y'}{\partial x} & \frac{\partial y'}{\partial y} & \frac{\partial y'}{\partial z} \\ \frac{\partial z'}{\partial x} & \frac{\partial z'}{\partial y} & \frac{\partial z'}{\partial z} \end{bmatrix} \{x\} \tag{4}$$

The rotational tensor $[R]$ is expressed in terms of the angles shown in Figure 3.1. In these coordinate systems, the z −axis is assumed to be on the $x' - y'$ plane.

$$[R_{ij}] = \begin{bmatrix} \sin\theta\cos\varphi & -\cos\theta\cos\varphi & \sin\varphi \\ \sin\theta\sin\varphi & -\cos\theta\sin\varphi & -\cos\varphi \\ \cos\theta & \sin\theta & 0 \end{bmatrix} \tag{5}$$

Then, the covariance kernel can be expressed in the non−prime coordinate system as

$$C(\overrightarrow{X_1}, \overrightarrow{X_2}) = \sigma^2 exp\left(-\frac{|x_1 - x_2|}{L_x} - \frac{|y_1 - y_2|}{L_y} - \frac{|z_1 - z_2|}{L_z} \right) \tag{6}$$

With this transformation, the correlation lengths can be specified in three arbitrary directions. Assigning different correlation lengths $L_x \neq L_y \neq L_z$ can enforce a direction−sensitive spatial correlation length in any arbitrary direction, i.e. θ and φ. This modification transforms the original isotropic covariance kernel to a new direction−dependent orthotropic covariance kernel

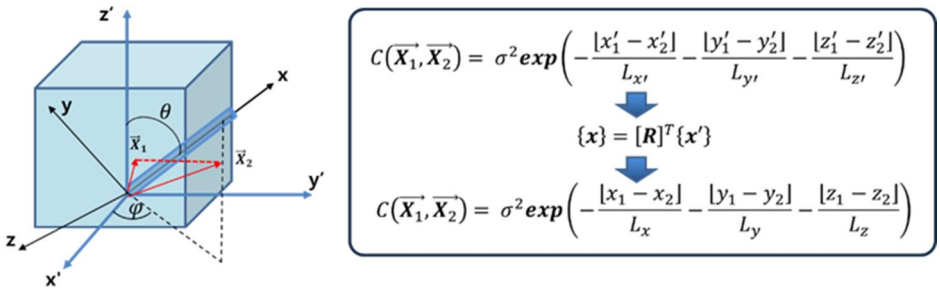

Figure 3.1 Rotational transformation of the covariance kernel function in an arbitrary direction

The Galerkin finite element method was used for discretization of the eigenfunction following the literature [65].

3.2. Mapping random fields to 3D finite mesh

The mesh size for the random field (RF) is related to the correlation length whereas the mesh size for the structural FE is related to the stress gradient. In this thesis, the generalized mapping method proposed in [65] is extended to a three-dimensional case by the algorithm illustrated in Figure 3.2.We implemented an 8-node brick finite element and 20-node brick finite element for a structural FE mesh and RF mesh, respectively.

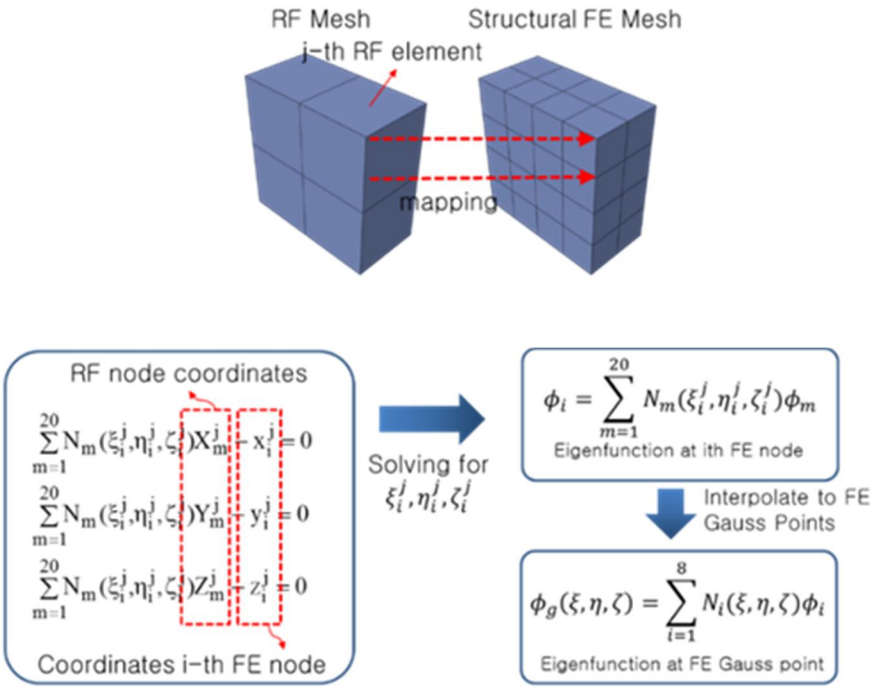

Figure 3.2 Generalized mapping eigenfunction values from the RF mesh to structural FE mesh nodal points

4. Linear Mori-Tanaka micromechanics model

In this section, we will provide a homogenization method, Mori-Tanaka method, to simulate the effective properties of CNT nanocomposites when matrix and inclusion are both elastic. In elasticity range, inclusion and matrix are follow constant effective properties so the strain-stress curve for single material or composites will be linear.

The original Mori-Tanaka is a commonly used homogenization method to develop accurate effective properties for composites. Ho wever, MT method has limitation when simulating complex situations. Instead of simulate straight, perfect fiber in matrix base, we derive an improved Mori-Tanaka method to simulate wavy CNT fiber with interfacial damage in matrix.

In this section, we will combine two improvements of classic MT homogenization and extend the simulation to orientation of inclusion in MT model. The improvement is, firstly, to introduce interfacial damage in original Mori-Tanaka method. And then, the second step

is to transform the straight CNT fiber into wavy model by using sinusoidal model.

4.1. MT model for CNT nanocomposites with interface damage

First, we consider the damage situation. We deal with the whole composites having only two phases, that is, matrix (0^{th} phase) and CNT (1^{st} phase). The CNT fiber as a sub-domain (Ω) is assumed as a long circular cylindrical inclusion in a homogenized matrix material (D). Original MT effective stiffness assumes unidirectional aligned inclusions. Homogeneous matrix subjected to uniform far-field applied strain (ε_a) shows the homogeneous strain field. However, the addition of inclusions causes perturbed inclusion strains and the average matrix strain $\langle\varepsilon_0\rangle$ is different from the average inclusion strain $\langle\varepsilon_1\rangle$ by the perturbed ε_1^{pt} inclusion strain as follows.

$$\langle\varepsilon_1\rangle = \langle\varepsilon_0\rangle + \varepsilon_1^{pt} = \langle\varepsilon_0\rangle + S\varepsilon_1^* \tag{7}$$

Where $\langle\ \cdot\ \rangle$ indicates values from volume averaging over the entire composite domain (D); ε_1^* is the fictitious eigenstrain of

inclusion in Ω; and S is the uniform 4^{th} order Eshelby inclusion tensor. The equivalent inclusion method can simulate inclusion stress $(\langle\varepsilon_1\rangle)$ by elastic stiffness (L_0) of the matrix and fictitious eigenstrain ε_1^* in Ω as follows. The relation between both coordinate system with rotational angle was shown in Figure 4.1. z' axis of material coordinate system aligns in x−y plane of a global coordinate system.

$$\varepsilon_1^* = -L_0^{-1}(L_1 - L_0)\langle\varepsilon_1\rangle \tag{8}$$

Substituting Equation (8) into Equation(7), we can derive the relationship between $\langle\varepsilon_1\rangle$ and $\langle\varepsilon_0\rangle$ with the dilute strain concentration tensor A_1 as follows.

$$\langle\varepsilon_1\rangle = A_1\langle\varepsilon_0\rangle = [I + SL_0^{-1}(L_1 - L_0)]^{-1}\langle\varepsilon_0\rangle \tag{9}$$

where I is the fourth order identity tensor. Equation (9) relates the average strain in the inclusion $\langle\varepsilon_1\rangle$ to the average strain in the matrix $\langle\varepsilon_0\rangle$ by the dilute strain concentration tensor. Accounting for the inclusion interaction, the applied strain for each inclusion is the average strain in the matrix $\langle\varepsilon_0\rangle$ instead of the far field applied strain(ε_0). This implies that we can write the average inclusion strain as follows

$$\langle \varepsilon_1 \rangle = A_1 \varepsilon_a \tag{10}$$

By the equal stress assumption $c_0\langle \varepsilon_0 \rangle + c_1\langle \varepsilon_1 \rangle = \varepsilon_a$, the average strain in the matrix is related to the applied strain as follows.

$$\langle \varepsilon_0 \rangle = A_0 \varepsilon_a = [c_0 I + c_1 A_1]^{-1} \varepsilon_a \tag{11}$$

Where c_0 and c_1 are the volume fractions of matrix and CNT, respectively. Then the effective elastic stiffness matrix of the MT model can be derived from the equal strain relationship $\langle \sigma_0 \rangle = c_0\langle \sigma_0 \rangle + c_1\langle \sigma_1 \rangle = L\varepsilon_a$ by substituting Hooke's law.

$$\begin{gathered} L = [c_0 L_0 + c_1 L_1 A_1][c_0 I + c_1 A_1]^{-1} \\ \text{Where} \quad A_1 = [I + S L_0^{-1}(L_1 - L_0)]^{-1} \end{gathered} \tag{12}$$

On the other hand, the Eshelby tensor for a long circular cylindrical fiber (i.e. CNT) is given as follows [66].

$$\begin{gathered} S_{1111} = S_{1122} = S_{1133} = 0 \\ S_{2222} = S_{3333} = \frac{5 - 4v_0}{8(1 - v_0)} \\ S_{2211} = S_{3311} = \frac{v_0}{2(1 - v_0)} \end{gathered} \tag{13}$$

$$S_{2233} = S_{3322} = \frac{4v_0 - 1}{8(1 - v_0)}$$

$$S_{1212} = S_{1313} = \frac{1}{4}$$

$$S_{2323} = \frac{v_0}{8(1 - v_0)}$$

Where v_0 is the poison ratio of the matrix. When calculating S_{ijkl}, Eshelby neglected the situation of interfacial debonding which means the perfect bonding between inclusions and matrix was assumed.

To consider imperfect interfacial bonding, a compliant spring layer with zero thickness is assumed to simulate continuous traction and discontinuous displacement along the interface as shown in Figure 4.1. MT modeling approach for weakened interfacial damage in a reference [58] was referred in this thesis.

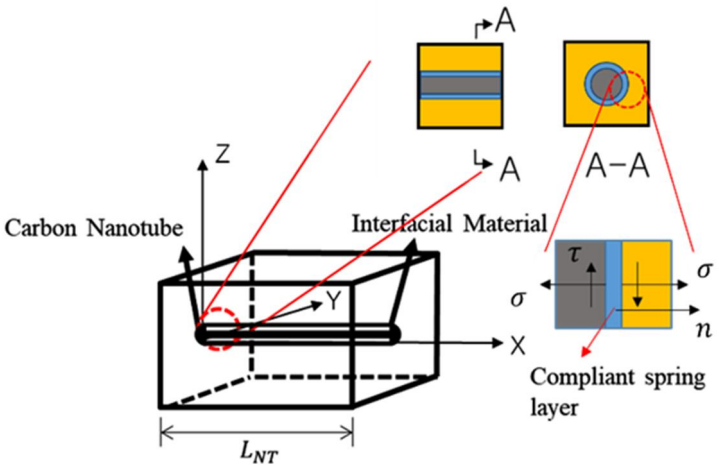

(a)

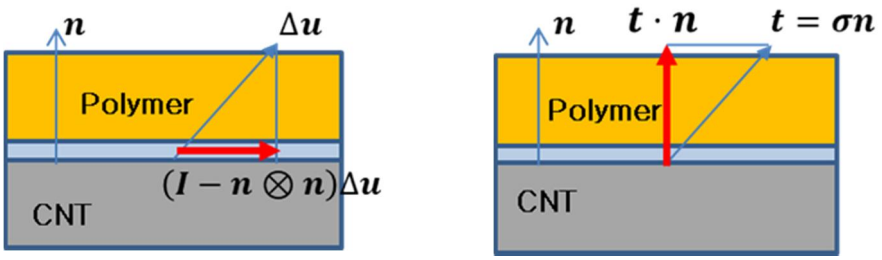

(b) **(c)**

Figure 4.1 (a) spring layer modeling of interphase (b) tangential component of discontinuous displacement (c) normal component of the traction

The compliance tensor for the single-layered interface is given as follows [58].

$$\eta = \alpha\delta_{ij}[e_i \otimes e_j] + (\beta - \alpha)n_i n_j[e_i \otimes e_j] \quad (14)$$

Where δ_{ij} is the Kronecker delta; η is the compliance tensor of the interface; and n_i is the outward normal vector to the interfacial surface between matrix and inclusion. α and β indicate compliance in the tangential and normal directions of the interface, respectively as defined in Equation (14).

$$(I - n \otimes n)\Delta u = \alpha(I - n \otimes n)\sigma n$$
$$\Delta u \cdot n = \beta \sigma n \cdot n \tag{15}$$

Where $(I - n \otimes n)$ is the projection tensor projected onto the interfacial surface; Δu is the displacement vector on the interface; $\sigma n (= t)$ is the traction vector by Cauchy stress formula; and I is the identity tensor. When $\eta_{ij} = 0$, there is no debonding between inclusion and matrix. When $\eta_{ij} \to \infty$ (i.e. zero stiffness), perfect debonding is applied.

In the case of imperfect interface, the inclusion strain field becomes non-uniform. By virtue of the Green's function in an infinite domain, the inclusion strain field with the weakened interface is obtained through modification of the original Eshelby solution [58, 67].

$$\varepsilon_{ij}(x) = S_{ijkl}\varepsilon_{kl}^{*} - L_{klmn}\int_{\partial\Omega}\eta_{kp}\sigma_{pk}(\xi)G_{ijmn}(\xi - n)n_q n_l dS(\xi) \qquad (16)$$

Where $\partial\Omega$ is the surface of the inclusion domain and G_{ijmn} is the function of the Green's function [58]. Certainly when $\eta_{kp} = 0$, the inclusion strain field becomes the original Eshelby equation and the inclusion strain is no longer uniform. Qu obtained the modified Eshelby tensor $\bar{S}_{ijkl}^{I}$ for the inclusion with the slightly weakened interface as follows [58].

$$\bar{S}^{I} = S + (I - S):H:L_0(I - S) \qquad (17)$$

Where L_0 is the effective stiffness of matrix material. H can be calculated in terms of the interfacial compliances as follows [58].

$$H_{ijkl} = \alpha P_{ijkl} + (\beta - \alpha)Q_{ijkl} \qquad (18)$$

Where P_{ijkl} and Q_{ijkl} are tensors that depend on the shape of inclusions. Original inclusion by Eshelby was an ellipsoidal shape of which domain is expressed by $\left(\frac{x_1}{a_1}\right)^2 + \left(\frac{x_2}{a_2}\right)^2 + \left(\frac{x_3}{a_3}\right)^2 \leq 1$, where a_1, a_2 and a_3 are principal semi-axes of ellipsoid. Ellipsoids can be specified to spherical and cylindrical inclusion shapes. In our case, inclusion is CNT fiber considered as a cylinder ($a_1 = a_2 = a$ and $a_3 \rightarrow$

∞) of which P and Q tensors are determined as follows [58], and here a is the radius of CNT inclusion. Having $a_3 \to \infty$ is the reason that the aspect ratio cannot be specified in the MT model, which will be explained later.

$$P_{1111} = P_{2222} = 4P_{2323} = 4P_{1313} = 2P_{1212} = \frac{3\pi}{8a}$$

$$Q_{1111} = Q_{2222} = 3Q_{1122} = 3Q_{2211} = 3Q_{1212} = \frac{9\pi}{32a} \qquad (19)$$

$$\text{Others}=0$$

Then the effective stiffness can be calculated for CNT reinforced nanocomposites with interfacial damage as follows [58].

$$\bar{L}^I = (c_0 L_0 + c_1 L_1 A_1^I)(c_0 I + c_1 A_1^I + c_1 H L_1 A_1^I)^{-1} \qquad (20)$$

Where A_1^I is the dilute strain concentration tensor for the weakened interface in inclusion phase. The dilute strain concentration tensor is obtained in terms of the modified Eshelby tensor in Equation(21).

$$A_1^I = [I + \bar{S}^I L_0^{-1}(L_1 - L_0)]^{-1} \qquad (21)$$

For the perfect bonding, α and β are zero and the tensor H becomes zero. Therefore, Equation (20) will become the original MT model.

4.2. MT model for wavy and interface weakened CNT Nanocomposite

After completing the strain concentration tensor A^I with interfacial damage, next is to derive the wavy CNT fiber,

An alternative form for the MT model can also be obtained as follows [37, 68]

$$L = L_0(I + c_1[(L_1 - L_0)^{-1}L_0 + c_0\bar{S}]^{-1}) \quad (22)$$

Where $\bar{S}$ is the Eshelby tensor that represents perfect interface bonding. Substituting the Eshelby tensor of Equation (17) into the alternative form of the MT Model in Equation(12), the effective elastic stiffness of composites with interface damage is obtained as follows.

$$\bar{L}^I = L_0(I + c_1[(L_1 - L_0)^{-1}L_0 + c_0\bar{S}^I]^{-1}) \quad (23)$$

Where $\bar{S}^I$ is the Eshelby tensor containing interface damage in Equation (17). This effective stiffness $\bar{L}^I$ was verified to provide the same elastic stiffness matrix as one from Equation(23) for a set of specific damage variables (i.e. α and β). We follow the analytical approach by Hsiao and Daniel [70] and Yanase et al. [69] in order to calculate the effective elastic stiffness of wavy CNT composites with interface weakened. Wavy CNT is modeled in a sinusoidal shape as depicted in Figure 4.2.

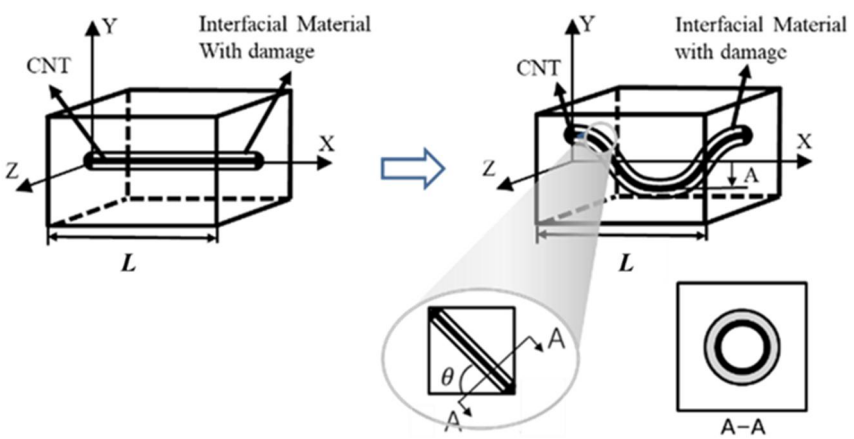

Figure 4.2 Modeling of wavy CNT fiber with interface damage

The sinusoidal waviness of CNT is defined in terms of the length L and amplitude A as follows.

$$v = A\sin\left(\frac{2\pi x}{L}\right)$$
$$a = \frac{2\pi A}{L} = 2\pi w \tag{24}$$

Where w is waviness. We applied a rotational transformation of $\bar{L}^I$ and averaged along the sinusoidal CNT fiber in order to obtain the effective stiffness $\bar{L}^{IW}$ of composites with interface weakened and wavy unidirectional CNT.

$$\bar{L}^{IW}_{\alpha\beta\gamma\delta} = \frac{1}{l}\int_0^l R_{i\alpha}R_{\beta j}R_{\gamma k}R_{\delta l}\bar{L}^I_{ijkl}dx$$
$$\text{Where } [R_{ij}] = \begin{bmatrix} \cos\theta & -\sin\theta & 0 \\ \sin\theta & \cos\theta & 0 \\ 0 & 0 & 1 \end{bmatrix} \tag{25}$$

Where θ is the tangential angle along the sinusoidal CNT as depicted in Figure 4.2. To conduct the averaging and rotational transforming in Equation (25) along a single inclusion fiber, we relate the angle θ to the waviness parameters A and L as follows.

$$\tan\theta = a\cos\frac{2\pi x}{L}$$

$$m = \cos\theta = \left[1 + \left(a\cos\frac{2\pi x}{L}\right)^2\right]^{-1/2} \tag{26}$$

$$n = \sin\theta = a\cos\frac{2\pi x}{L}\left[1 + \left(a\cos\frac{2\pi x}{L}\right)^2\right]^{-1/2}$$

The integration in Equation (25) can be explicitly expressed as

$$\frac{1}{L}\int_0^L m^4 dx = \frac{2 + a^2}{2(1 + a^2)^{3/2}} = I_1$$

$$\frac{1}{L}\int_0^L m^2 n^2 dx = \frac{a^2}{2(1 + a^2)^{1/2}} = I_2$$

$$\frac{1}{L}\int_0^L m^2 dx = \frac{1}{(1 + a^2)^{1/2}} = I_1 + I_2 \tag{27}$$

$$\frac{1}{L}\int_0^L n^2 dx = 1 - \frac{1}{(1 + a^2)^{3/2}} = 1 - I_1 - I_2$$

$$\frac{1}{L}\int_0^L m^3 n dx = \frac{1}{L}\int_0^L m n^3 dx = \frac{1}{L}\int_0^L mn dx = 0$$

Components of the transformed stiffness matrix in Equation (20) are expressed explicitly as follows

$$\bar{L}^{IW}_{1111} = I_1(\bar{L}^{I}_{1111} - \bar{L}^{I}_{2222}) + 2I_2(\bar{L}^{I}_{1122} - \bar{L}^{I}_{2222} + 2\bar{L}^{I}_{1212}) + \bar{L}^{I}_{2222}$$

$$\bar{L}^{IW}_{1122} = I_2(\bar{L}^{I}_{1111} - 2\bar{L}^{I}_{1122} + \bar{L}^{I}_{2222} - 4\bar{L}^{I}_{1212}) + \bar{L}^{I}_{1122}$$

$$\bar{L}^{IW}_{1133} = I_1(\bar{L}^{I}_{1122} - \bar{L}^{I}_{2233}) + I_2(\bar{L}^{I}_{1122} - \bar{L}^{I}_{2233}) + \bar{L}^{I}_{2233}$$

$$\bar{L}^{IW}_{2211} = I_1(\bar{L}^{I}_{1111} - 2\bar{L}^{I}_{1122} + \bar{L}^{I}_{2222} - 4\bar{L}^{I}_{1212}) + \bar{L}^{I}_{1122}$$

$$\bar{L}^{IW}_{2222} = I_1(\bar{L}^{I}_{2222} - \bar{L}^{I}_{1111}) + I_2(2\bar{L}^{I}_{1122} - 4\bar{L}^{I}_{1212} - 2\bar{L}^{I}_{1111}) + \bar{L}^{I}_{1111}$$

$$\bar{L}^{IW}_{2233} = I_1(\bar{L}^{I}_{2233} - \bar{L}^{I}_{1122}) + I_2(\bar{L}^{I}_{2233} - \bar{L}^{I}_{1122}) + \bar{L}^{I}_{1122}$$

$$\bar{L}^{IW}_{3311} = (I_1 + I_2)(\bar{L}^{I}_{1122} - \bar{L}^{I}_{2233}) + \bar{L}^{I}_{2233} \tag{28}$$

$$\bar{L}^{IW}_{3322} = (I_1 + I_2)(\bar{L}^{I}_{2233} - \bar{L}^{I}_{1122}) + \bar{L}^{I}_{1122}$$

$$\bar{L}^{IW}_{3333} = \bar{L}^{I}_{3333}$$

$$\bar{L}^{IW}_{1212} = I_2(\bar{L}^{I}_{1111} - 2\bar{L}^{I}_{1122} + \bar{L}^{I}_{2222} - 4\bar{L}^{I}_{1212}) + \bar{L}^{I}_{1212}$$

$$\bar{L}^{IW}_{2323} = (I_1 + I_2)(\bar{L}^{I}_{2323} - \bar{L}^{I}_{1212}) + \bar{L}^{I}_{1212}$$

$$\bar{L}^{IW}_{1313} = (I_1 + I_2)(\bar{L}^{I}_{1212} - \bar{L}^{I}_{2323}) + \bar{L}^{I}_{2323}$$

Substituting $\bar{L}^{IW}$ of Equation (28) into $\bar{L}^{I}$ of Equation(23), we can obtain the MT model for wavy CNT nanocomposites with interface damage as follows.

$$\bar{L}^{IW} = L_0(I + c_1[(L_1 - L_0)^{-1} + c_0\bar{S}^{IW}]^{-1}) \tag{29}$$

Then the Eshelby tensor $\bar{S}^{I}$ changes to $\bar{S}^{IW}$ accordingly. The Eshelby tensor $\bar{S}^{IW}$ is for CNT inclusions with both interfacial damage and waviness. Then, we can back-calculate the Eshelby tensor $\bar{S}^{IW}$ for wavy CNT with interface damage as follows

$$\bar{S}^{IW} = \lim_{c_1 \to \infty} \frac{1}{1-c_1}\left[c_1\left({L_0}^{-1}\bar{L}^{IW} - I\right)^{-1} - (L_1 - L_0)^{-1}L_0\right] \tag{30}$$

Applying the modified Eshelby tensor in Equation(30), we can also obtain the effective elastic stiffness as follows.

$$\begin{aligned} \bar{L}^{IW} &= (c_0 L_0 + c_1 L_1 A_1^{IW})(c_0 I + c_1 A_1^{IW})^{-1} \\ A_I^{IW} &= [I + \bar{S}^{IW} L_0^{-1}(L_1 - L_0)]^{-1} \end{aligned} \tag{31}$$

An alternative form for the effective stiffness of wavy CNT nanocomposites with interface weakened is also introduced as follows

$$\begin{aligned} \bar{L}^{IW} &= (c_0 L_0 + c_1 L_1 A_1^{W})(c_0 I + c_1 A_1^{W} + c_1 H L_1 A_1^{W})^{-1} \\ A_1^{W} &= [I + \bar{S}^{W} L_0^{-1}(L_1 - L_0)]^{-1} \end{aligned} \tag{32}$$

Where

$$\bar{S}^{W} = \lim_{c_1 \to \infty} \frac{1}{1-c_1}[c_1(L_0^{-1}\bar{L}^{W} - I)^{-1} - (L_1 - L_0)^{-1}L_0]$$

According to our tests, effective stiffness matrices of Equation. (31) and (32) are identical. These MT models are for unidirectional aligned CNT nanocomposites as shown in Figure 4.3(a). However, in most cases, actual CNT fibers are randomly oriented as in Figure 4.3(b). Therefore, in the following section, an efficient modeling approach for 3D randomly orientated CNT nanocomposites is presented

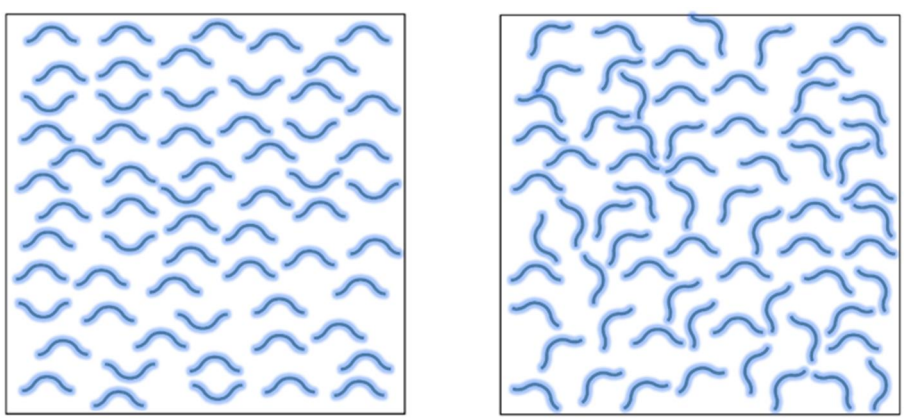

(a) **(b)**

Figure 4.3 (a) unidirectional aligned wavy CNT distribution (b) randomly oriented wavy CNT distribution

4.3. Modeling of orientation for CNT nanocomposites

In this thesis, we will model two kinds of common orientation modeling. One is aligned model with stochastic fiber orientation and the other is 3D randomly oriented modeling.

First is stochastic aligned model. Classical deterministic micromechanics models are transformed to probabilistic ones using the direction-sensitive 3D KLE method. All variables followed by (x, ω) are spatially random field quantities.

The proposed method models the stochastically-aligned 3D CNT nanocomposites by treating two orientation angles (i.e. θ_{CNT} and φ_{CNT}) of the CNT fibers as spatially varying random fields. By the KLE method, they are expressed as

$$\theta_{CNT}(x', y', z', \omega) = \langle \theta_{CNT} \rangle + \sum_{i=1}^{m} \sqrt{\lambda_i} \phi_{\theta_i}(x', y', z') \left[\xi_{\theta_i}(\omega) \right]$$
$$\varphi_{CNT}(x', y', z', \omega) = \langle \varphi_{CNT} \rangle + \sum_{i=1}^{m} \sqrt{\lambda_i} \phi_{\varphi_i}(x', y', z') \left[\xi_{\varphi_i}(\omega) \right] \quad (33)$$

where $< \cdot >$ is the mean value; ω is the primitive randomness; ξ is the normal variable; λ and ϕ are the eigenvalue and eigenfunction

of the assumed analytical covariance kernel, respectively; m is the truncation order of the KLE. The mean values of the angles and the correlation length in the (x, y, z) directions are the main statistical parameters factors that determine stochastic orientations of the CNT. Even if we manufacture aligned CNT nanocomposites by using a mechanical and electrical method [71], every CNT fiber in real polymer matrix cannot be perfectly aligned, as is illustrated in Figure 4.4. Therefore, the aligned CNT nanocomposites hold spatially varying anisotropic properties.

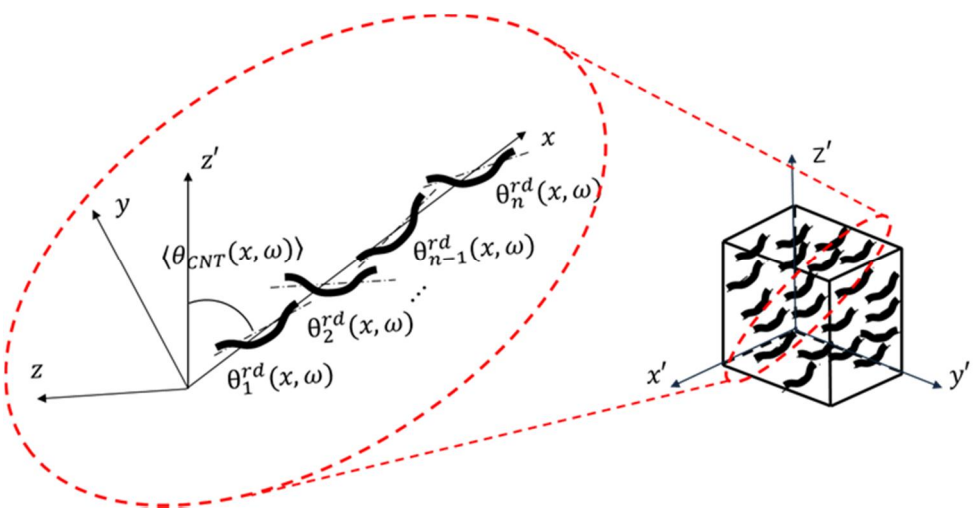

Figure 4.4 Spatially varying random aligned angles with $\langle\theta_{CNT}\rangle$: mean and θ_i^{rd}: random fluctuations

The stress and strain tensors are transformed back and forth between the prime system $(x' - y' - z')$ and non−prime system $(x - y - z)$ as follows

$$\sigma'_{\alpha\beta} = R_{\alpha i} R_{\beta j} \sigma_{ij}$$
$$\varepsilon_{\alpha\beta} = R_{i\alpha} R_{j\beta} \varepsilon'_{ij} \tag{34}$$

The random rotational tensor is expressed in terms of the angles in Equation (35) as

$$\left[R_{ij}(x, \omega)\right] = \begin{bmatrix} \sin\theta_{CNT}\cos\varphi_{CNT} & -\cos\theta_{CNT}\cos\varphi_{CNT} & \sin\varphi_{CNT} \\ \sin\theta_{CNT}\sin\varphi_{CNT} & -\cos\theta_{CNT}\sin\varphi_{CNT} & -\cos\varphi_{CNT} \\ \cos\theta_{CNT} & \sin\theta_{CNT} & 0 \end{bmatrix} \tag{35}$$

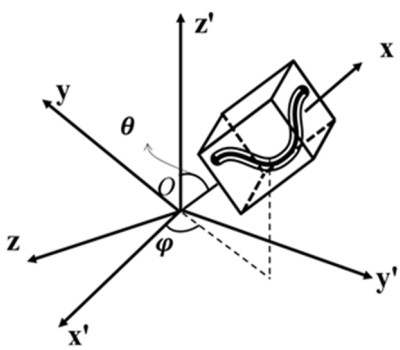

Figure 4.5 A spatial oriented CNT fiber with Euler angles

Although $[R]$ in Equation (5) takes the same form as Equation (35), they are used differently. $[R]$ in Equation (5) is a deterministic rotational transformation tensor for the covariance kernel but $[R(x,\omega)]$ in Equatioan (35) is a random one for stresses and strains. Assuming the linear elastic Hooke's law, the 4^{th} stiffness tensors are also transformed as

$$\sigma'_{\alpha\beta} = R_{\alpha i}R_{\beta j}R_{\gamma k}R_{\delta l}C_{ijkl}\varepsilon'_{\gamma\delta}$$
$$C'_{\alpha\beta\gamma\delta}(x,\omega) = R_{\alpha i}R_{\beta j}R_{\gamma k}R_{\delta l}C_{ijkl} \quad (36)$$

where C_{ijkl} is the elasticity tensor in the non-prime system. C_{ijkl} is computed by using engineering constants from micromechanical models we described in section 2.

Then, comes to 3D randomly oriented simulation.

In typical CNT nanocomposites, the reinforcing CNT fibers are not perfectly aligned but randomly oriented in the three-dimensional space. This three-dimensional random orientation of CNT fibers results in quasi-isotropic effective stiffness of the composites. For 3D randomly oriented CNT nanocomposites, rotational averaging of the fourth order tensors is required. We applied a method to realize

3D randomly orientation averaging of the fourth order tensor proposed in literature [14]. In this method, the effective stiffness is computed through orientation averaging on L_1A_1 and A_1 as follows.

$$\bar{L}^{IW} = (c_0 L_0 + c_1 \langle L_1 A_1^{IW} \rangle_\theta)(c_0 I + c_1 \langle A_1^{IW} \rangle_\theta)^{-1}$$
$$A_1^{IW} = [I + \bar{S}^{IW} L_0^{-1}(L_1 - L_0)]^{-1} \tag{37}$$

where $\langle \cdot \rangle_\theta$ indicates the orientation average of the corresponding tensors. The simplified direct formula for the orientation averaging can be written as follows [14].

$$W = M_\theta$$

$$W_{11} = \frac{1}{15}(8M_{11} + 2M_{12} + 2M_{31} + 3M_{33} + 4\zeta M_{44})$$
$$W_{12} = \frac{1}{15}(M_{11} + 5M_{12} + 4M_{13} + 4M_{31} + M_{33} - 2\zeta M_{44}) \tag{38}$$

$$W_{44} = \frac{1}{\zeta}(M_{11} - M_{12})$$

This is different components for $\langle L_1 A_1 \rangle_\theta, \zeta = 1$ and $\langle A_1 \rangle_\theta, \zeta = 2$, and other components in the matrix are determined as follows.

$$W_{11} = W_{22} = W_{33} \tag{39}$$

$$W_{12} = W_{21} = W_{13} = W_{31} = W_{23} = W_{32}$$

$$W_{44} = W_{55} = W_{66}$$

This approach is equivalent to the method in [16]. These formulae are originated from the orientation average of a fourth-order tensor given by $\langle M_{ijkl} \rangle_\theta = \left(\frac{1}{a}\right) \int_\Omega Q_{ip} Q_{jq} Q_{kr} Q_{ls} d\Omega$. Here, Q_{ij} is the appropriate rotational transformation tensor. The orientation averaging is conducted according to the general framework from literature [72].

5. Nonlinear Mori-Tanaka micromechanics model

In Section 4, we introduced an improved method to simulate CNT nanocomposites in elastic range. However, we also need to consider the situation that plasticity occurs. When plasticity occurs, the strain–stress curve is nonlinear and plastic effective properties is related to hardening function, plastic strain and ductile damage.

Hence, elasto–plastic properties have always been one of most interested properties of composites. Researchers are attracted in elasto–plasticity not only to simulate the material properties after composites damage, but also it is more realistic in research experiment and production. Azoti [73] et al, provided an elasto–plastic constitutive model with incremental micromechanics scheme. We have further research in modeling of plasticity of CNT nanocomposites with interface and ductile damage in matrix phase since damage is inevitable element in simulations.

In Section 5, we will introduce a nonlinear composites model in plastic range, with using Mori–Tanaka method with interfacial

damage and ductile damage is introduced by using Lemaitre–Chaboche damage modeling method. Also, since the effective properties difference of matrix and inclusion is usually great, so we assume the inclusion is always elastic during the simulation while matrix will become plastic with increasing of strain. On the other hand, multiscale transformation is proposed to achieve macro stress and strain increment.

5.1. Iterative update of global strain concentration tensor

For CNT nanocomposites, we consider two phases, CNT inclusion and polymer matrix and boundary condition and kinematic loadings are in macro scope.

Global strain concentration tensor A is defined by Equation (40) and links local strain with macroscopic strain E

$$e(r) = A(r) : E \tag{40}$$

Dederichs and Zeller [74] provided the kinematic integral equation as

$$\varepsilon(r) = E^R(r) - \int_V \Gamma(r - r') : \delta c(r') dV \tag{41}$$

where $\varepsilon(r)$ is the local strain, $\Gamma(r - r')$ is the modified Green tensor and E^R is the strain field in the reference infinite medium. Also $c(r')$ indicates the local effective stiffness, and the integration is over the Representative Volume Element (RVE) with volume V.

Then we can get

$$\varepsilon^I(r) = a^I(r) : E^R \tag{42}$$

where $a^I(r)$ is the local strain concentration tensor which relates the local stress with strain field in the reference medium. Based on the theory proposed by Vieville [75], the global strain concentration tensor is

$$A^I(r) = a^I(r) : (\bar{a}^I)^{-1} \tag{43}$$

where $\bar{a}^I$ is the volume mean local concentration tensor which in two-phase composites with interfacial damage can be expressed as

$$\bar{a}^I = c_0 a^0 + c_1 a^1 + c_1 H^1 L_1 a^1$$
$$A^0 = (\bar{a}^I)^{-1} \tag{44}$$

where H^1 is the interfacial damage tensor we mentioned in Section 4, And c_0 and c_1 are the volume fraction of inclusion and matrix, respectively.

In our case of one site simulation, local strain concentration a^I is given as

$$a^I = [I + S:(L_0)^{-1}:(L_1 - L_0)]^{-1} \tag{45}$$

In this equation, I is the identity tensor, S is the Eshelby tensor and L_1 and L_0 are the microscopic stiffness tensor for inclusion and resin, respectively.

Hence, substituting Equation (45) into Equation. (43) we can get the global concentration tensor A^I as

$$A^I = [I + S:(L_0)^{-1}:(L_1 - L_0)]^{-1}:[c_0 a^0 + c_1 a^1 + c_1 H^1 L_1 a^I]^{-1} \tag{46}$$

5.2. Ductile damage plasticity for polymer resin

5.2.1. Flow rules with damages

In this process, we introduce J_2 flow rule to determine whether matrix is elastic or plastic, while CNT inclusion is assumed always being elastic because of great effective properties. And in elastic or plastic situation, we update hardening scalar r, accumulated plastic strain p, ductile damage D, micro stress σ and micro plastic strain ε^p respectively.

The flow rule function is provided as follows.

$$f = \sigma_e^{trial} - 3G\Delta p - R(r) - \sigma_{y0} \tag{47}$$

Where $R(r) = kr^m$ nonlinear isotropic hardening function is described by the scalar variable r. And k and m in the hardening function are material properties and σ_{y0} in the equation is the yield stress and $\sigma_e^{\text{trial}}$is the equivalent trial stress.

The equivalent trial stress is defined as

$$\hat{\sigma}_e^{trial} = L^{el} : \left[(\varepsilon_n + \Delta\varepsilon) - \varepsilon_n^p\right] \tag{48}$$

The subscript e means equivalence of stress which follow the equation

$$\sigma_e = J_2(\hat{\sigma}) = \left[\frac{3}{2}(\hat{s}):(\hat{s})\right]^{\frac{1}{2}} \tag{49}$$

In the equation, s is deviatoric stress which can be calculated by

$$\hat{s} = \hat{\sigma} - \frac{1}{3}(tr\hat{\sigma})1 \tag{50}$$

To deal with multivariate Newton's Iteration, we first to note several relationships.

The flow rule can also been expressed as

$$f_{\hat{\sigma}} \equiv \hat{\sigma}_e - \hat{\sigma}_e^{trial} + 3G\Delta p \tag{51}$$

All the stress and strain variable with $(\hat{\cdot})$ means accounting in the revolution of ductile damage which specifically represents

$$(\hat{\cdot}) = \frac{(\cdot)}{1-D} \tag{52}$$

The basic of flow rule is to simulate material is in the state of elastic or plastic. Following the Equation (47) we can judge the state by

$$\begin{cases} elastic, f \leq 0 \\ plastic, f > 0 \end{cases} \tag{53}$$

If $f \leq 0$, it means that the prediction is correct, so

$$\begin{gathered} \hat{\sigma}_{n+1} = \hat{\sigma}_{n+1}^{trial} \\ \left(r_{n+1}, p_{n+1}, D_{n+1}, \varepsilon_{n+1}^{p}\right) = \left(r_n, p_n, D_n, \varepsilon_n^{p}\right) \end{gathered} \tag{54}$$

On the other hand, if $f > 0$, which represents the equivalent trial stress $\hat{\sigma}_e^{trial}$ is larger than the sum of yield stress and hardening stress, and the assumption is incorrect that means plasticity occurs and we need to find a $\hat{\sigma}_{n+1}$ which can make $f = 0$. This process is called plastic corrector.

Since the relationship of

$$\hat{\sigma}_{n+1} = \hat{\sigma}_{n+1}^{trial} - L^{el} : \Delta\varepsilon^{p} \tag{55}$$

And because of the $\Delta\varepsilon^{p}$ is deviatoric, the Equation (55) becomes

$$\hat{\sigma}_{n+1} = \hat{\sigma}_{n+1}^{trial} - 2G\Delta\varepsilon^{p} \tag{56}$$

Now the problem becomes to solve the unknown $\Delta\varepsilon^{p}$. And we introduce the vector$N$, which is normal to flow rule f.

$$N \equiv \frac{\partial f}{\partial \sigma} = \left(\frac{3}{2}\right)\frac{s}{J_2(\sigma)} \tag{57}$$

Then we simply need to find Δp instead of $\Delta \varepsilon^p$ since

$$\Delta \varepsilon^p = N \Delta p \tag{58}$$

5.2.2. Algorithmic tangent operator

In previous section, we have derived the updated micro stress $\hat{\sigma}_{n+1}$. Then we can calculate effective stiffness of ductile matrix $\hat{L}^{alg}$ at $n+1$ iteration

$$\delta \hat{\sigma}_{n+1} = \hat{L}^{alg} \delta \hat{\varepsilon}_{n+1} \tag{59}$$

Where

$$\hat{C}^{alg} = \hat{C}^{ep} - (2G)^2 \frac{\Delta p}{[1+(\frac{3}{2})g]} \frac{\partial^2 f}{\partial \hat{\sigma} \partial \hat{\sigma}}$$

$$\hat{L}^{alg} = \hat{L}^{ep} - (2G)^2 \frac{\Delta p}{\left[1 + \left(\frac{3}{2}\right) g\right]} \frac{\partial^2 f}{\partial \hat{\sigma} \partial \hat{\sigma}} \tag{60}$$

$$\hat{L}^{ep} = L^{el} - (2G)^2 \frac{\hat{N} \otimes \hat{N}}{h}$$

$$h = 3G + \frac{\partial R}{\partial r}$$

$$g = \frac{2G\Delta p}{\hat{\sigma}} > 0$$

$$\frac{\partial^2 f}{\partial \hat{\sigma} \partial \hat{\sigma}} = \frac{1}{\hat{\sigma}_e}\left(\frac{3}{2} I^{dev} - \hat{N} \otimes \hat{N}\right)$$

And then we can get the local stiffness tensor as

$$L^{alg} = (1 - D)\hat{L}^{alg} \tag{61}$$

It is noted that, we introduce mid-point rule at $n + \alpha$ to improve the accuracy. We use effective stiffness at $n + 1$ and new calculated deriving $\hat{L}^{alg}_{n+\alpha}$ as figure shown.

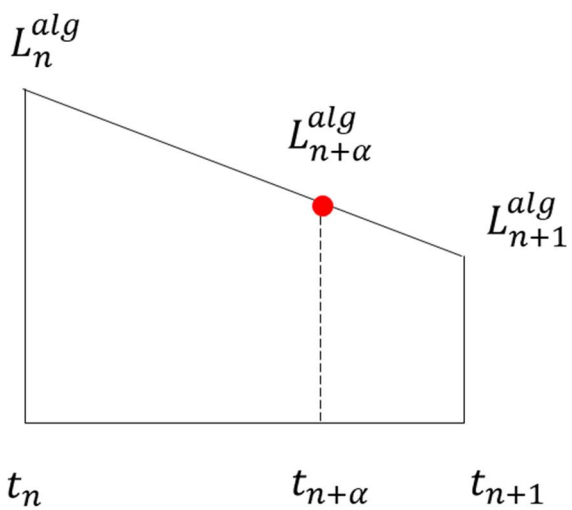

Figure 5.1 Scheme of Mid-Point Rule

$$L_{n+\alpha}^{alg} = (1-\alpha)L_n^{alg} + \alpha L_{n+1}^{alg} \tag{62}$$

The equation is shown for both inclusion and matrix when calculating algorithmic tangent operator.

5.3. Fully implicit update of internal variables

5.3.1. Return mapping algorithm

It is more complicated when we consider the situation of damage comparing with no ductile damage case at the same time. We need to satisfy three equations instead of one and to update three unknown variables in the meantime.

$$\begin{cases} f_{\hat{\sigma}} \equiv \hat{\sigma}_e - \hat{\sigma}_e^{trial} + 3G\Delta p = 0 \\ f_f \equiv J_2(\hat{\sigma}) - R(r) - \sigma_{y0} = 0 \\ f_D \equiv \Delta D - y(\hat{\sigma})\dfrac{\Delta r}{1-D} \end{cases} \tag{63}$$

In the equation, $y(\hat{\sigma})$ is shorten notation which is related to strain energy release Y.

$$y = \left(\frac{Y}{S_0}\right)^s$$

$$Y = \frac{1}{2E}\left(\frac{\hat{\sigma}_e}{1-D}\right)^2 R_v$$

$$R_v = \frac{2}{3}(1+v) + 3(1-2v)\left(\frac{\hat{\sigma}_H}{\hat{\sigma}_e}\right)^2 \tag{64}$$

$$\hat{\sigma}_H = \frac{\hat{\sigma}_{kk}}{3}$$

Where s is a material properties and here is set to be 0.5.

We set the unknown variables are $\begin{Bmatrix} \Delta\hat{\sigma} \\ \Delta r \\ \Delta D \end{Bmatrix}$. Following Newton's iteration

$$x_{i+1} = x_i - \frac{f(x_i)}{\frac{\partial f}{\partial x}} \tag{65}$$

So for multivariate Newton's iteration, we derive a Jacobian matrix

$$\begin{Bmatrix}\Delta\hat{\sigma}\\ \Delta r\\ \Delta D\end{Bmatrix}^{(k+1)} = \begin{Bmatrix}\Delta\hat{\sigma}\\ \Delta r\\ \Delta D\end{Bmatrix}^{(k)}$$

$$-\begin{bmatrix} I + 2G\frac{\partial N^{tr}}{\partial\hat{\sigma}}\Delta p^{(k)} & \frac{2GN^{tr}}{1-D_n} & \frac{2GN^{tr}}{1-D_n}\Delta p^{(k)} \\ (N^{tr})^T & -\left(\frac{\partial R}{\partial r}\right)^{(k)} - \frac{3G}{1-D_n} & \frac{3G\Delta p^{(k)}}{1-D_n} \\ -\Delta p^{(k)}\left(\frac{\partial y}{\partial\hat{\sigma}}\right)^{(k)^T} & -\frac{y^{(k)}}{1-D_n} & 1-\frac{y^{(k)}\Delta p^{(k)}}{1-D_n} \end{bmatrix} \begin{Bmatrix} f_{\hat{\sigma}} \\ f_r \\ f_D \end{Bmatrix}^{(k)} \qquad (66)$$

$$\Delta p^{(k+1)} = \frac{\Delta r^{(k+1)}}{1-D_n}$$

In the equation, the partial derivative is calculated by

$$\frac{\partial N^{tr}}{\partial\hat{\sigma}} = \frac{1}{J_2\left(\hat{\sigma}'^{tr}\right)}\left(\frac{3}{2}I - \hat{N}\otimes\hat{N}\right)$$

$$\frac{\partial R}{\partial r} = hm(r)^{m-1} \qquad (67)$$

$$\frac{\partial y}{\partial\hat{\sigma}} = \frac{\partial y}{\partial\hat{\sigma}_{ij}} = \frac{\partial y}{\partial\hat{\sigma}'_{ij}} = \frac{s}{S_0^s}\left[\frac{(1+\nu)\hat{\sigma}'_{ij}\hat{\sigma}'_{ij}}{2E(1-D_n)^2} + \frac{(1-2\nu)\hat{\sigma}_{pp}}{6E(1-D_n)^2}\right]^{s-1}\left[\frac{(1+\nu)\hat{\sigma}'_{ij}}{E(1-D_n)^2} + \frac{(1-2\nu)\hat{\sigma}_{pp}\delta_{ij}}{3E(1-D_n)^2}\right]^{s-1}$$

The main scheme is depicted as Figure 5.2 shown. From known n iteration stress $\hat{\sigma}_n$, we first assume trial stress $\hat{\sigma}_n^{trial}$, and then through Newton iteration, we do internal iteration to find a new stress which is close to real value.

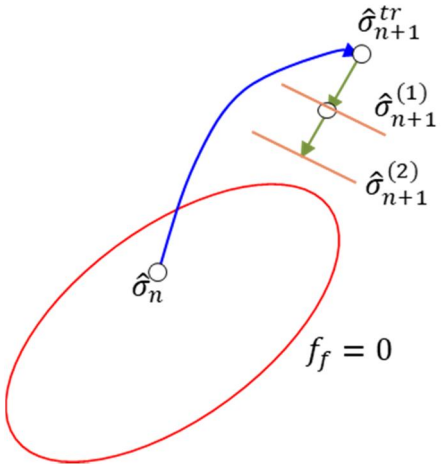

Figure 5.2 Return Mapping Algorithm

5.3.2. Numerical implementation

It is noted that the fully implicit Newton Raphson's iteration is operated in the t_n to t_{n+1} time domain, so when updating global concentration tensor A^I, in the outer iteration, Newton Raphson's iteration will still in the time domain $[t_n, t_{n+1}]$

Hence, from Equation (66), we can solve Newton's iteration and get

$$\hat{\sigma}_{n+1} = \hat{\sigma}_n + \Delta\hat{\sigma}^{(k+1)} \tag{68}$$

$$r_{n+1} = r_n + \Delta r^{(k+1)}$$

$$D_{n+1} = D_n + \Delta D^{(k+1)}$$

$$\Delta\, p^{(k+1)} = \frac{\Delta r^{(k+1)}}{1-D_n}$$

The overall Newton iteration is shown as

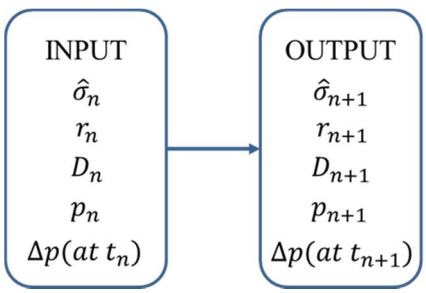

Figure 5.3 In & Output of Newton Raphson's Iteration

After Newton Raphson's iteration, the updated $\hat{\sigma}, r, D$ and Δp

Satisfy the three equations in Equation (63)

Figure 5.4 shows the convergent condition of fully implicit Newton Raphson's iteration. The iteration convergent quickly in first several iterations which indicates the Newton iteration is working well.

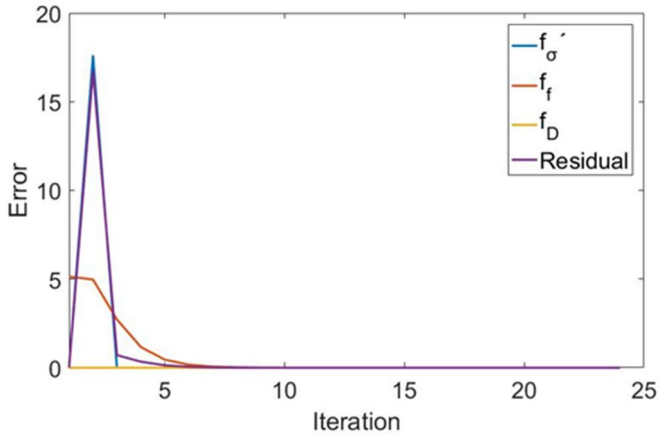

Figure 5.4 Convergent of multivariable Newton Iteration

5.4. Overall algorithm for nonlinear MT model

To evaluate plasticity, we first use scale transition techniques, from macro to micro, and achieve constitutive properties of matrix and inclusion respectively. We first initialize a macro stress increment and initial identity strain concentration tensor A^I .

Then we can get micro strain increment with Equation(69), for inclusion and matrix respectively

$$\Delta\varepsilon^I = A^I_{old} : \Delta E$$
$$\Delta\varepsilon^0 = \frac{\Delta E - c_1 \Delta\varepsilon^I}{1 - c_1} \tag{69}$$

In the equation, superscript I and 0 means inclusion and matrix phase respectively. ΔE is macro strain increment which can be set in advance. And c_1 is volume fraction of inclusion.

And then we can calculate stress increment in microscale

$$\sigma = (1 - D)L^{el} : (\varepsilon - \varepsilon^p) \tag{70}$$

Where D is variable which describes ductile damage. D=0 represents no damage in matrix. In the equation, $\boldsymbol{\varepsilon}$ is microscale strain, ε^p is micro plastic strain and L^{el} is elastic stiffness of material.

It is noted that $D = \frac{A_D}{A_0}$, where A_D and A_0 are the area of damage and the total area respectively.

Also, we have relationship between r, p and D as shown

$$\dot{r} = (1 - D)\dot{p} \tag{71}$$

Where r is hardening function scalar and p is accumulated plastic strain.

Then following section 5.2 and 5.3, we can calculate the updated stress and get algorithm tangent operator for inclusion and matrix respectively.

After we get effective stiffness $\hat{L}_{n+\alpha}^{alg}$ for fiber and matrix, in the microscale, we can get strain concentration tensor with interfacial damage as Equation (29) shows. And based on Equation (45) the macroscale concentration tensor A^I can be derived from

$$A^I = a^I : A^0 \tag{72}$$

Here, subscript I and 0 indicate inclusion and matrix phase respectively, and lowercase a means local microscale strain concentration tensor and capital A is global strain concentration tensor. Where A^0 is, and L_1 is effective stiffness calculated from Equation(73).

$$A^0 = (c_0 I + c_1 a^I + c_1 H^1 : L_1 : a^I)^{-1} \tag{73}$$

After getting new A^I, we need to check the residual which is

$$R = A^I : \Delta E - \Delta \varepsilon^I \tag{74}$$

If the residual is, we can continue to the Mori-Tanaka homogenization and finally derive macro strain from

$$\Delta \Sigma = L^{MT} : \Delta E \tag{75}$$

Otherwise, we need to update A^I and repeat the simulation from Equation(69).

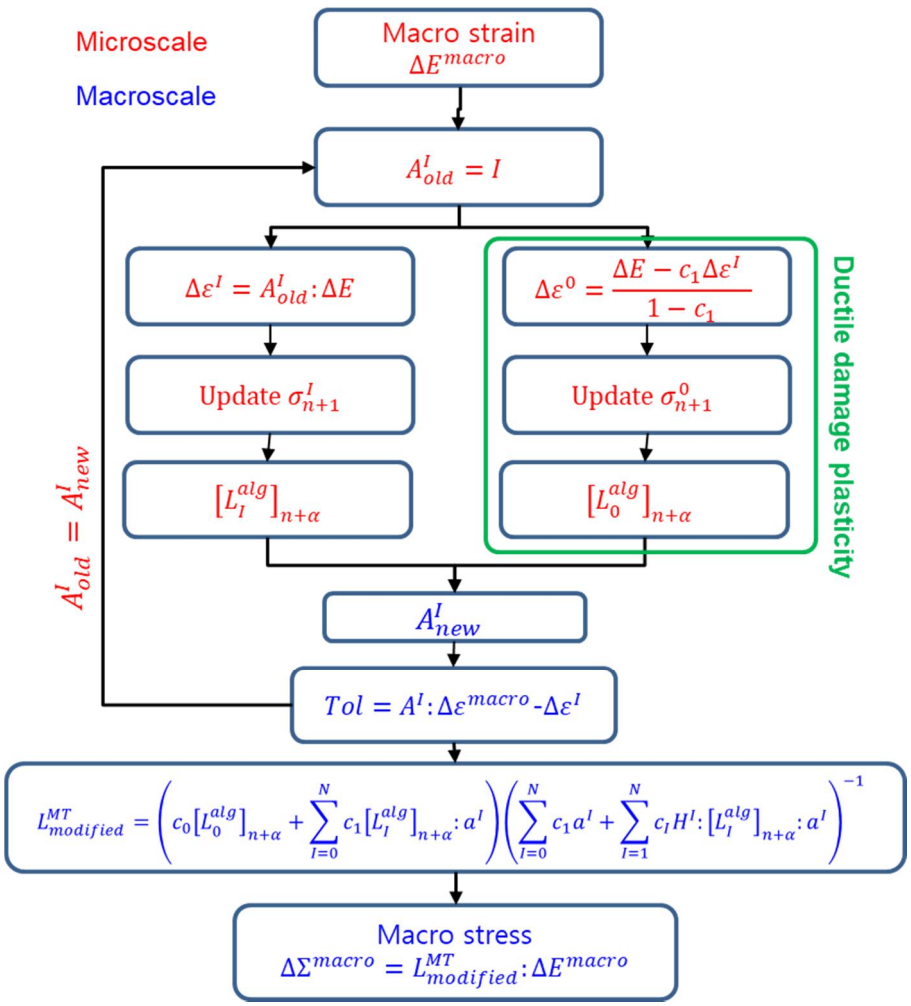

Figure 5.5 Scheme of Mori-Tanaka Model

The whole scheme is shown as Figure 5.5

6. Numerical examples

6.1. Effects of material properties

Figure 6.1 shows the effective Young's modulus versus volume fraction of the present model and experimental data. Experiment data are based on properties of MWNT (multi-walled nanotube)/polystyrene composites [76]. We did not distinguish the single-walled CNT from multi-walled CNT. Assumed material properties are summarized in Table 6-1. For modeling, 3D fully random orientation was assumed with waviness w=0.1. Interfacial damage parameters $\alpha = 0.1163$ and $\beta = 0.0332$ were computed using the formulae from [58].

$$\alpha = \frac{t}{G_i}$$

$$\beta = \frac{t}{K_i + \frac{4}{3}G_i} \tag{76}$$

Where t is the thickness of the interphase region; G_i and K_i are the shear and bulk moduli of the interphase region, respectively. Properties of the interphase region from the literature [77]. The

thickness of the interphase region was 0.17 nm. The present model shows good predictions of the experimental curve although SWNT (single-walled nanotube) was assumed. The error of Figure 6.1 increases with the increment of volume fraction, the biggest error is 10.2%. Since the experiment cannot precisely measure the orientation, waviness and damage of CNT composites, and these uncertainties of composites properties in experiment affect greatly. So, we can verify the validity of our simulation with experiment.

Table 6-1 Elastic properties of CNT-polystyrene composites

	Matrix	CNT inclusion
Young's Modulus(GPa)	1.9	1000
Shear Modulus(GPa)	0.731	384.62
Poisson Ratio	0.3	0.3
Waviness (w=A/L)	–	0.1

Interfacial Damage [38]	–	α=0.1163, β=0.0332

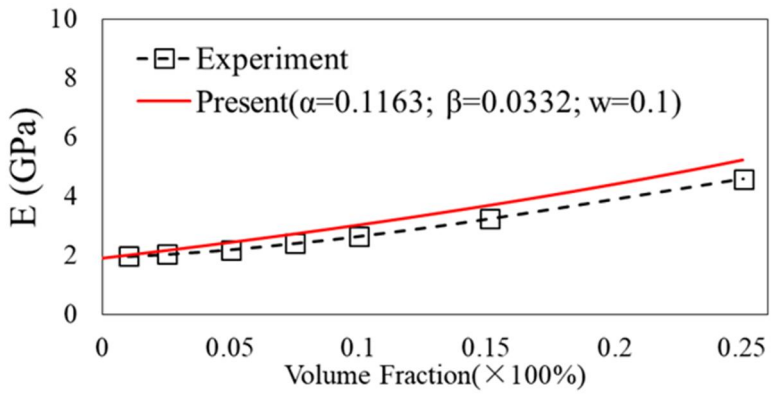

Figure 6.1 Comparison of the experiment [76] and present models for wavy and interface-damage CNT

Figure 6.2 shows the effects of CNT waviness and different combinations of interfacial damage to the effective Young's modulus. For waviness, w=0.1. For shear interfacial damage only, α=0.1 and β=0.0. For normal damage only, α=0.0 and β=0.1. Blue spots in Figure 12 apply both shear and normal damages at the same time, which are specifically α=0.1 and β=0.1. Stiffness drop was more attributed to the interfacial damage than the waviness. In the case of interfacial damage, stiffness drop due to the waviness was minimal, since the largest stiffness drop due to the interfacial damage was observed in the case of straight CNT. In the meanwhile, interfacial

damages applied both on shear and normal directions reduce Young's modulus of nanocomposites.

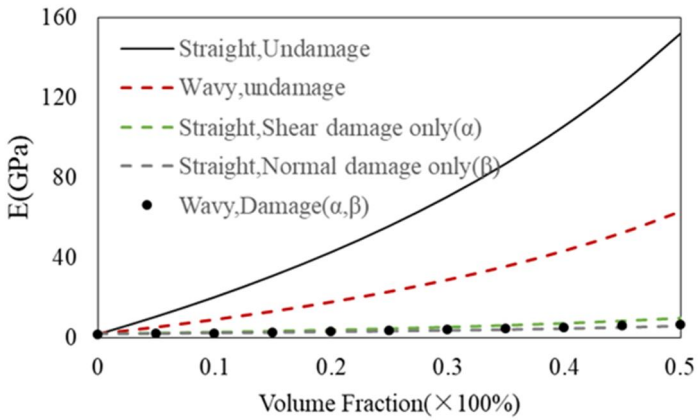

Figure 6.2 Effective Young's modulus of CNT nanocomposites versus volume fraction with various combination of waviness and interfacial damage

Figure 6.3 shows the effective Young's modulus versus volume fraction with different waviness and comparisons with experiment results from literature [69]. For interface damage, α=0.1163 and β=0.0332. In Figure 6.3(a), it is shown the comparison of experiment results and method presented in this thesis. It clearly indicates the similarities both on tendency and values. And Figure 6.3 (b) proves that if assuming original interfacial damages previously, elastic properties will drop greatly.

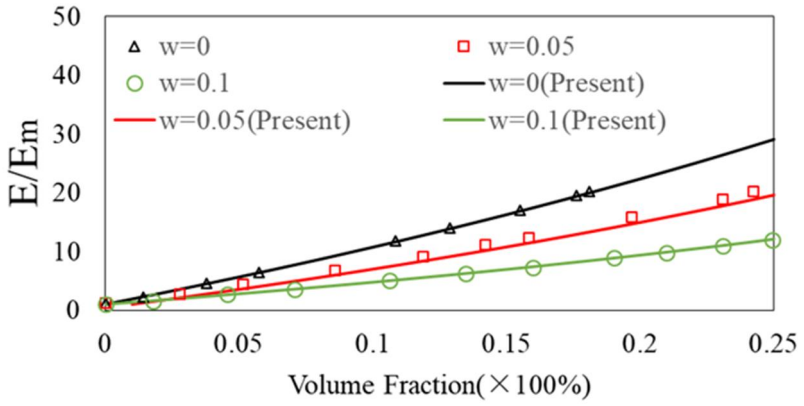

(a)

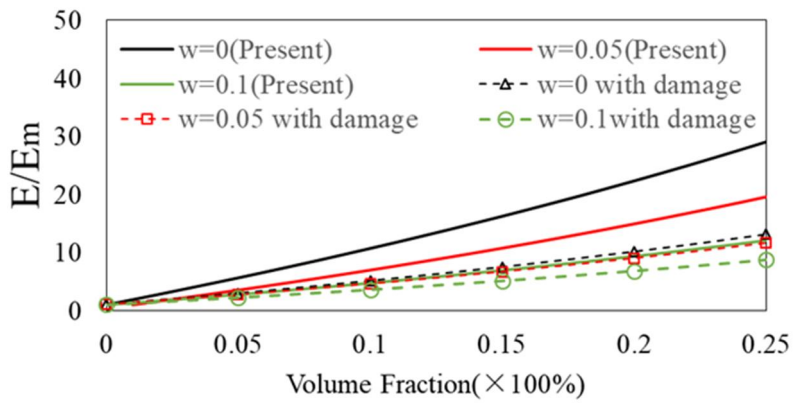

(b)

Figure 6.3 Effective Young's modulus ratio with various waviness

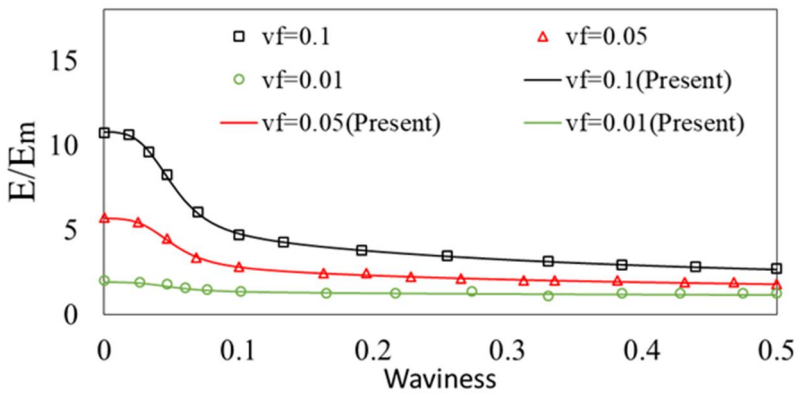

(a)

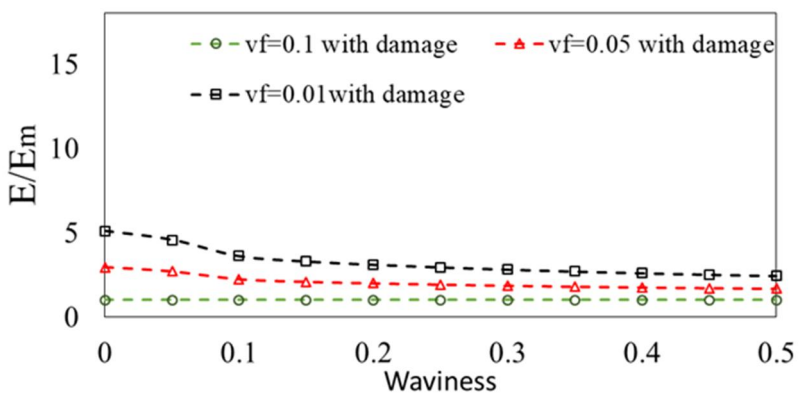

(b)

Figure 6.4 Effective Young's modulus ratio without interface damage v.s. waviness with various volume fractions and effects of interface damage

Figure 6.4 obviously indicates that effective Young's modulus decreases with increment of the waviness and decrement of the volume fraction. In the case of perfect bonding, the present model shows good agreement with results from the literature [69]. The effective Young's modulus drastically drops when the waviness is larger than around 0.04 and smaller than 0.2, which presents that effective stiffness is sensitive in this waviness range. When the waviness becomes larger than 0.2, the influence of waviness will decrease. For damage case, we assumed α=0.1163 and β=0.0332. Certainly, the interface damage reduces the effective Young's modulus.

6.2. Effects of spatial orientation of composites

6.2.1. 3D stochastically aligned CNT nanocomposites

Table 6-2 includes the assumed base material properties in section 6.2. CNT properties of the multi-walled nanotubes are assumed, and this is acceptable for the current micromechanics

model. The matrix properties from [15] are for a typical polymer matrix.

Table 6-2 Properties of applied materials

CNT [28,29]		Matrix Material [15]		Interfacial Material	
α	0.1	E_m	1.9 GPa	E_i1)	5.0 GPa
E_{cnt1}	1.58 TPa	ν_m	0.3	d_i2)	1.7 nm
ν_{cnt12}	0.156	G_m	0.73 GPa	d_{CNT}3)	1.36 nm
G_{cnt12}	0.493 TPa			1) [30]; 2) [31]; 3) [29]	

The three random fields are assumed to have lognormal distributions. Following references, we selected the mean and

standard deviation values that not only maintain random values lying in a valid range, but also controls variations to consider the effect of waviness and interfacial phase reasonably.

Table 6-3 Statistic parameter of random fields

(⟨ ⟩: mean, σ : std, L: correlation length)

	Volume fraction v_{CNT} [32]		Waviness α [28]		Interfacial Material E_i [33]
$\langle v_{CNT} \rangle$	0.125	$\langle \alpha \rangle$	0.1	$\langle E_i \rangle$	5.0 GPa
$\sigma_{v_{CNT}}$	0.25	σ_α	0.1	σ_{E_i}	1.0
$L_{v_{CNT}}$	20 nm	L_α	20 nm	L_{E_i}	20 nm

Unlike randomly-oriented CNT nanocomposites, stochastically-aligned 3D CNT nanocomposites have anisotropic material properties. The random angles θ_{CNT}[zf1]and $\varphi_{CNT}$are assumed to have normal distributions. The statistical parameters for these simulations are tabulated in Table 6-4. However, the volume fraction of the CNT and waviness are assumed to have deterministic values of 0.125 and 0.1, respectively. We intended to simulate and show how stochastically aligned angles induce anisotropy of elastic properties. Therefore, we randomize only the aligned angles, θ_{CNT} and φ_{CNT}.

Table 6-4 Statistical parameter to simulate the CNT nanocomposites ($\langle\theta_{CNT}\rangle = 90°, \langle\varphi_{CNT}\rangle = 5°$)

Random Variables	θ_{CNT}	φ_{CNT}
Mean	90°	5°
Std	0.1	0.1
Correlation length in x, y, z direction	$L_1 = 6\mu m$ $L_2 = L_3 = 20nm$	$L_1 = 6\mu m$ $L_2 = L_3 = 20nm$

The distributions of nine engineering constants computed from Equation (33) appear to be random, as shown in Figure 4.5. Since the longitudinal direction of the CNT is aligned to 1', $E_{1'}$ the values are larger than $E_{2'}$ and $E_{3'}$. Moreover, because of the longer correlation length in the 1' direction than 2' and 3' directions, the level of fluctuation in 1' direction is less than one in other directions.

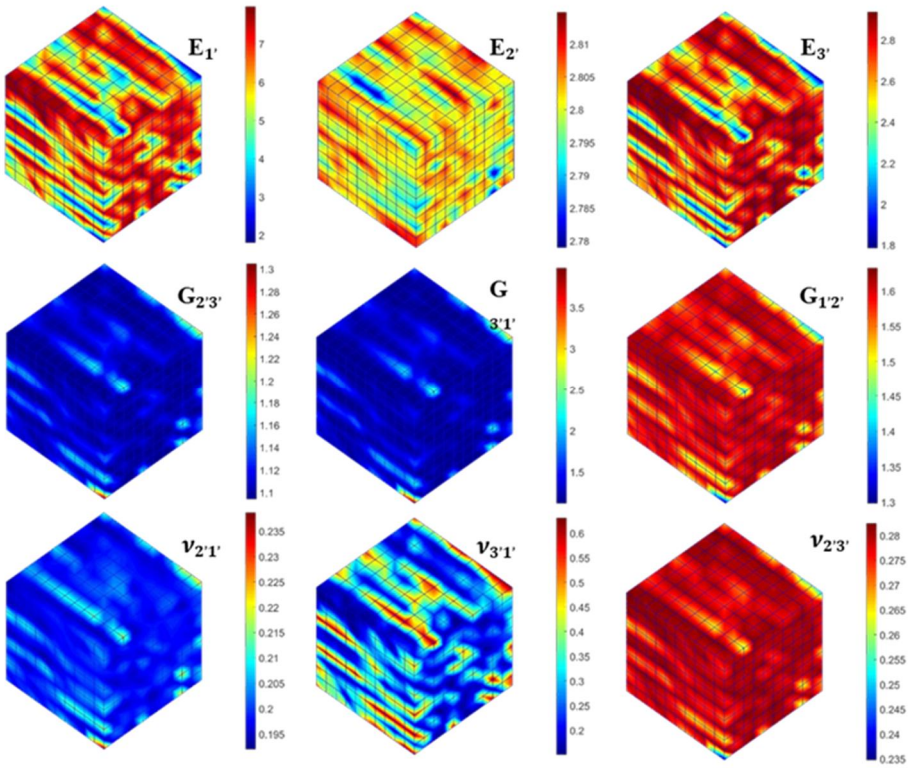

Figure 6.5 One realization of nine engineering constants for aligned CNT nanocomposites with ($\langle\theta_{CNT}\rangle = 90°$,$\langle\varphi_{CNT}\rangle = 5°$)

For further demonstration of the effects of the CNT orientation and correlation lengths on random distributions of the engineering constants, we assume different statistical parameters in Table 6−5

Table 6-5 Statistical parameter for aligned CNT nanocomposites ($\langle\theta_{CNT}\rangle = 45°, \langle\varphi_{CNT}\rangle = 0°$)

Random Variables	θ_{CNT}	φ_{CNT}
Mean	45°	0°
Std	0.5	0.5
Correlation length in x, y, z direction	$L_1 = 100\mu m$ $L_2 = L_3 = 20nm$	$L_1 = 100\mu m$ $L_2 = L_3 = 20nm$

Figure 6.6 illustrates random distributions of the nine engineering constants in the 1′−2′−3′ coordinate system. From Figure 6.6, we notice that the engineering constants vary smoothly along the diagonal direction on the 1′−3′ plane whereas they show greater fluctuations in the normal direction than in the diagonal direction. As demonstrated, the proposed modeling method has an obvious advantage in that it can realistically (i.e., not perfectly aligned) model aligned CNT nanocomposites with physically well−defined probabilistic parameters.

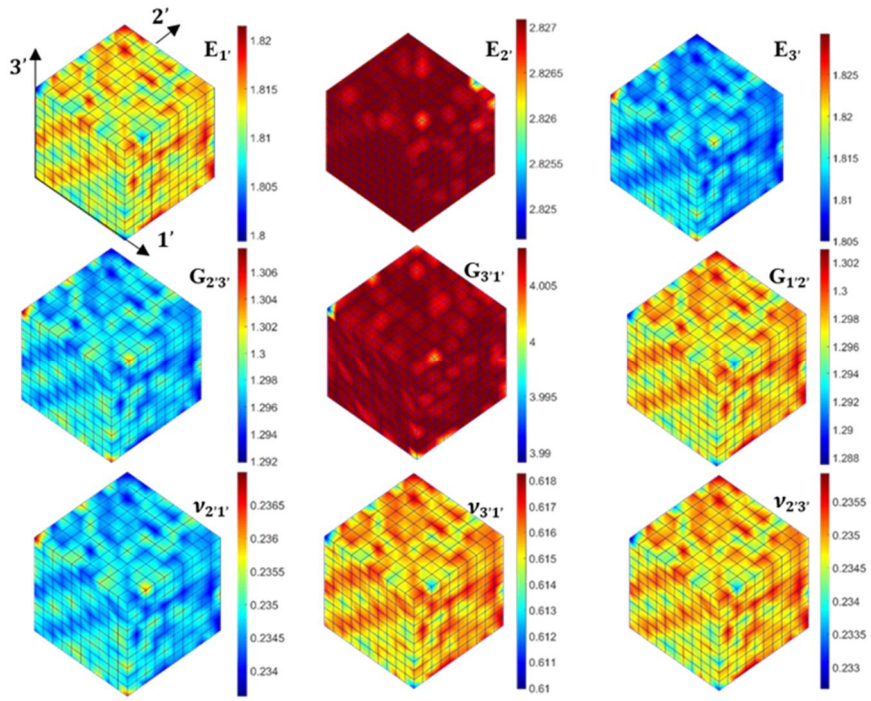

Figure 6.6 One realization of nine engineering constants for aligned CNT nanocomposites with ($\langle\theta_{CNT}\rangle = 45°$,$\langle\varphi_{CNT}\rangle = 0°$)

6.2.2. 3D randomly oriented CNT nanocomposites

In this simulation, the microscale RVE size made of CNT-embedded epoxy is 12 μm x 12 μm x 12 μm. Assuming no interfacial stiffness, we realize random distributions of elastic stiffness within this RVE. A total of 1000 8-node brick finite elements are used for the realizations. The number of the RF elements is 125.

To compare the effects of the random volume fraction, waviness, and interfacial stiffness, two combinations of random fields are simulated using the Monte Carlo sampling method, that is, $\alpha - v_{CNT}$ and $E_i - v_{CNT}$. Probabilistic ranges in Figure 6.7 (a) and (b) indicate the effects of random waviness and random interfacial stiffness at each local volume fraction, respectively. In the case of $\alpha - v_{CNT}$, experimental data are slightly off from the range. Our results well matched with the experiment data showing similar tendency. The little discrepancy between our simulation results and experiment data is mainly caused by modelling simplification and randomness of the waviness, interfacial property and local volume fraction. In the case of $E_i - v_{CNT}$,the effect of interfacial stiffness is observed to be marginal. Therefore, the effective modulus of randomly-oriented 3D CNT nanocomposites is more sensitive to waviness than the interfacial stiffness. In this simulation, our purpose is to identify the dominant parameter among the two parameters. Therefore, we only considered two random parameters per each case. We assume no specific correlation between the interfacial stiffness, waviness and volume fraction.

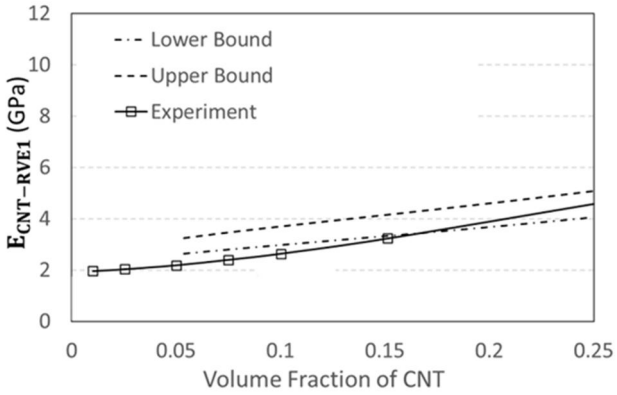

(a)

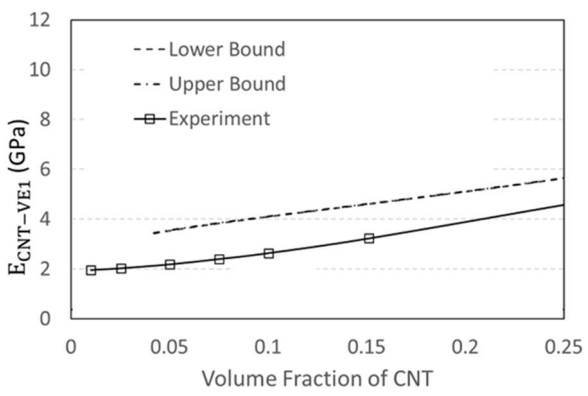

(b)

Figure 6.7 (a) Random waviness and volume fraction (b) random interfacial stiffness and volume fraction effects on the effective modulus $E_{CNT-VE1}$ Experiment: [76]

As illustrated in Figure 6.8, the isosurfaces of $E_{CNT-VE1}$ indicate truly random local elastic modulus due to only random local CNT volume fractions. The difference between VE1 and VE2 is VE2 have two matrix caps on left and right side of VE1. So VE2 has smaller volume fraction of CNT than VE1. The local volume fraction $v_{CNT}(x,\omega)$ in Equation (33) is dependent on the location x. Random local volume fractions form non-uniform dispersion of CNT fillers. When we generate random local volume fraction $v_{CNT}(x,\omega)$, local volume fraction is spatially varying within the random field space. Higher local volume fraction indicates more agglomerated CNT fillers at the location x. Random distributions of the effective elastic modulus in Figure 6.8 are caused by the random local volume fraction, that is, non-uniform dispersion.

When we generate random local volume fraction, the local elastic stiffness in Figure 6.8(a) and (b) assume a 20 nm correlation length in all x, y, and z directions and Figure 6.8(c) and (d) 6 μm in all x, y, and z directions. As shown in Figure 6.8, a smaller correlation length appears to have a more fluctuating distribution. According to this result, effects of the correlation length seem to be very significant.

Therefore, a method of experimentally measuring the correlation length can be briefly described as follows. At an array of fixed discrete points in the micro region, nano-indentation tests can be conducted to obtain a set of physical properties from multiple samples at each of the discrete points. After that, a discrete covariance matrix can be obtained and by fitting the discrete correlation coefficient to the analytical covariance function, we can estimate the correlation lengths defined in the analytical covariance function.

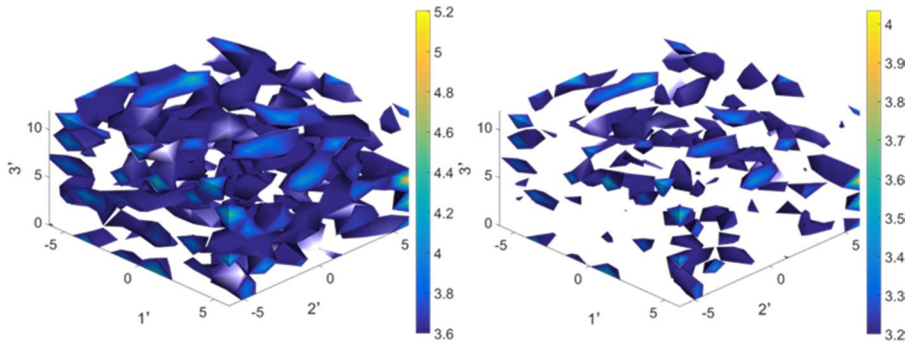

(a) Elastic Modulus of VE1 ($E_{CNT-VE1}$=3.6)

(b) Elastic Modulus of VE2 ($E_{CNT-VE2}$=3.2)

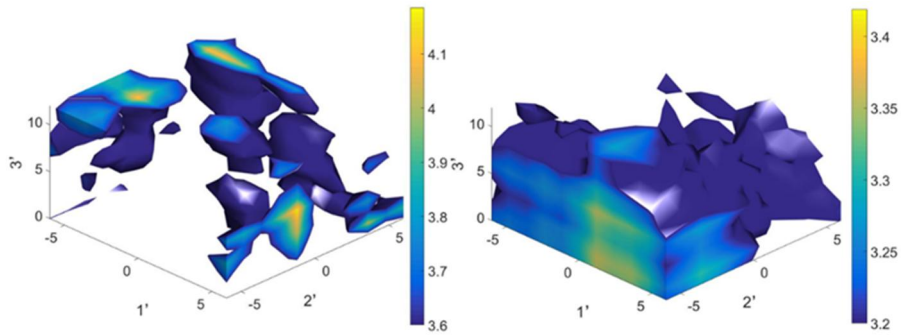

(c) Elastic Modulus of VE1 ($E_{CNT-VE1}$=3.6)

(d) Elastic Modulus of VE2 ($E_{CNT-VE2}$=3.2)

Figure 6.8 Random distributions of elastic modulus of 3D randomly oriented CNT nanocomposites within microscale RVE (a) VE1 random local volume fraction ($L_x = L_y = L_z = 20nm$) (b) VE2 random local volume fraction ($L_x = L_y = L_z = 20nm$) (c) VE1 random volume fraction ($L_x = L_y = L_z = 6\mu m$) (d) VE2 random local volume fraction ($L_x = L_y = L_z = 6\mu m$)

6.3. Effects of interfacial damage

Figure 6.9 shows a variation of effective Young's modulus with varying damage parameters α and β. Here in Figure 14, waviness w=0.1 and volume fraction of CNT is 0.1. The rate of changes of the stiffness was lessened as the damage parameters become larger. Also, we notice that the stiffness seems to be more sensitive to the normal damage (β) than the shear interfacial damage (α).

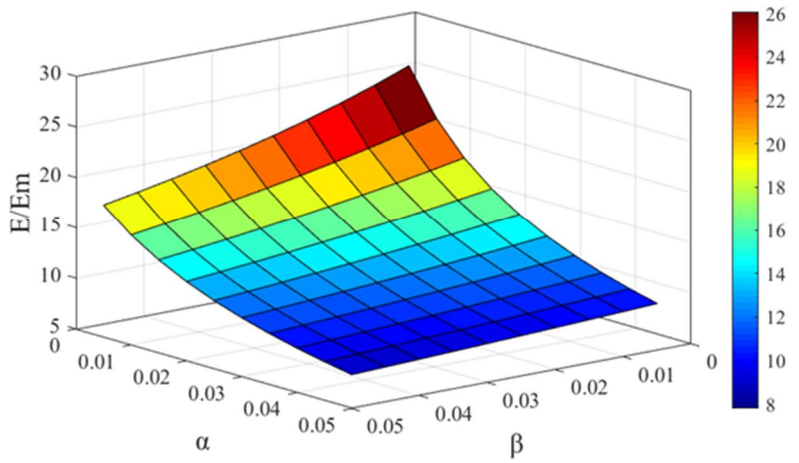

Figure 6.9 Effective properties with various interface damage

Figure 6.10 indicates the effective Young's moduli (E_1 and E_3) of 3D aligned CNT nanocomposites as one of the aligned angle φ varies and the waviness changes. The other Euler angle θ is fixed at 90 degree. The waviness a=0.1 and volume fraction equals to 0.1. For damage case, α=0.1163 and β=0.0332. Young's modulus (E_1) in the longitudinal direction is sensitive to both the orientation and waviness, whereas Young's modulus (E_3) in the transverse direction is insensitive to the orientation changes by the angle φ. Figure 6.10 shows damage parameter indeed having a negative effect on effective

properties and the influence will become smaller when the damage parameter become larger.

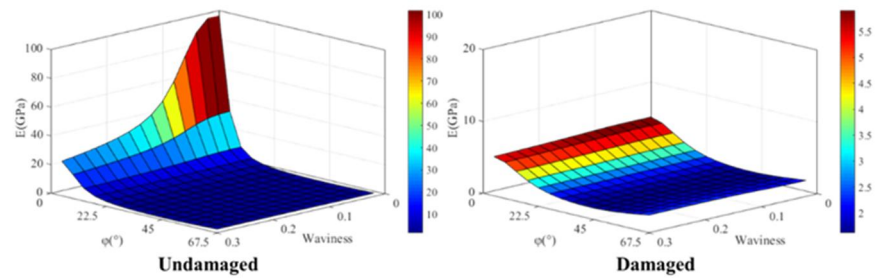

(a)

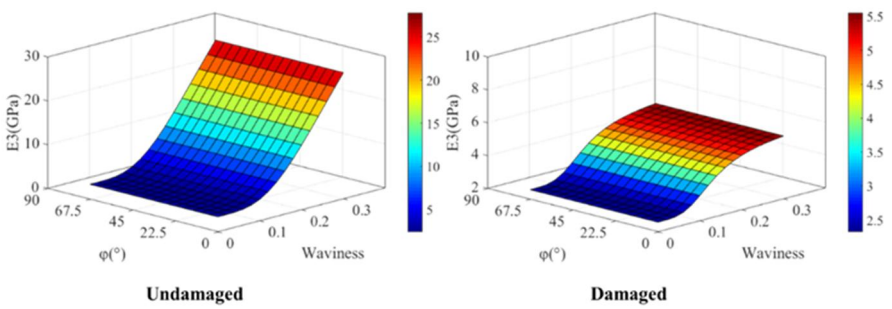

(b)

Figure 6.10 (a) Longitudinal and (b) transverse effective Young's modulus with varying orientation, waviness and damage parameter α and β

6.4. Effects of ductile damage

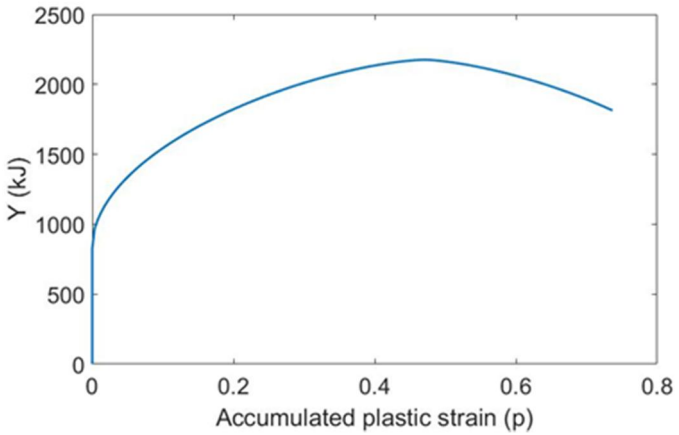

Figure 6.11 The effect of *p* on strain release energy *Y*

Figure 6.11 gives the relationship of accumulated plastic strain and strain energy release. From the very beginning of plastic occurrence, large amount of energy released and the rate of increment become smaller with the evolution of p.

Material properties used in Figure 6.11 to Figure 6.19 are based on Table 6-6.

Table 6-6 Material properties of plasticity simulation

	Matrix	Inclusion
Young's Modulus	2GPa	1000GPa

Poisson Ratio	0.39	0.22
Yield stress	60.5MPa	–
Hardening Function	$h = 63MPa$ $m = 0.4$	–

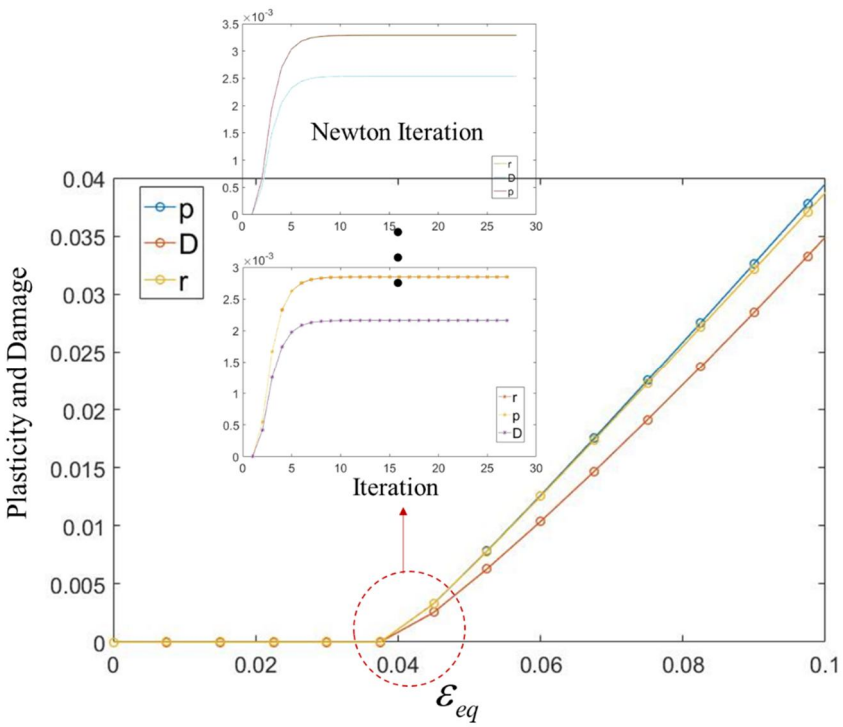

Figure 6.12 Iteration of Newton's and strain increment

Figure 6.12 gives the Newton's iteration and macro strain increase process. It is noted that, Newton's iteration runs several

time to update global strain concentration tensor A^I. So, every time when Newton iteration is running, it will start from same time point until A^I convergent.

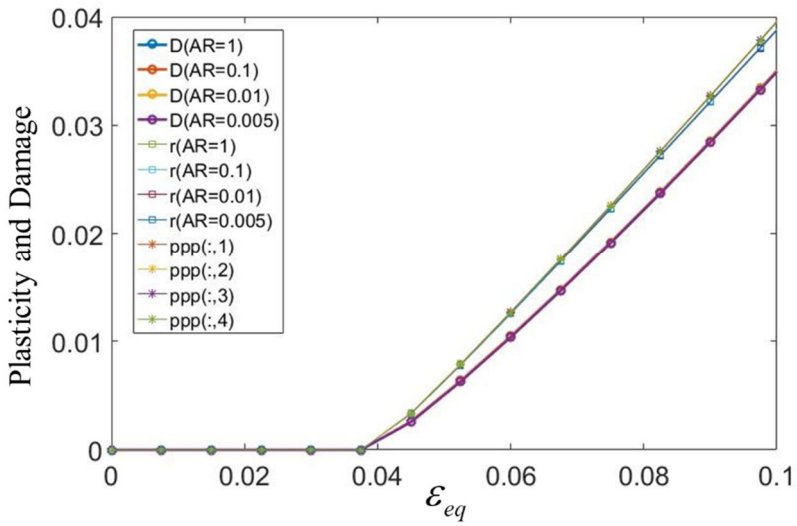

Figure 6.13 Plasticity and damage evolution with various aspect ratio

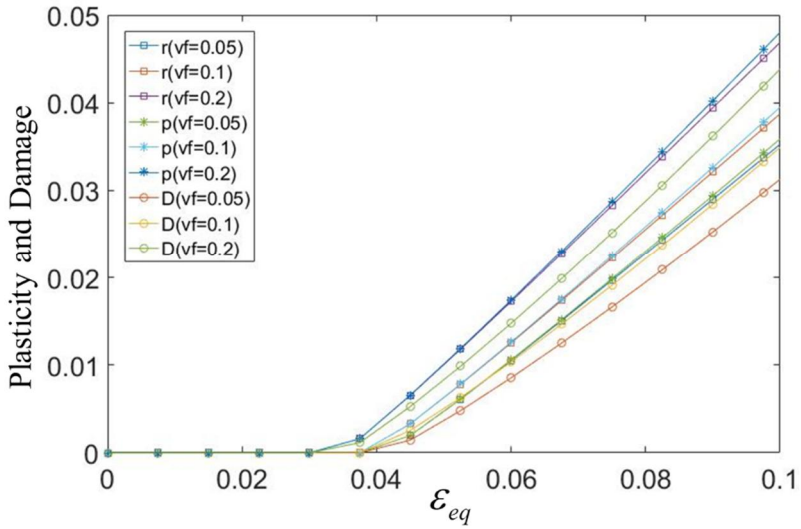

Figure 6.14 The influence of volume fraction on plastic and damage evolution

In the Figure 6.13, accumulated plastic strain, ductile damage, and hardening scalar have few relationship with aspect ratio which indicates the shape of inclusion has little influence on damage evolution. In the meanwhile, we can see ductile damage is smaller than p and r. In the case of without considering ductile damage, r and p are defined to have same value. And since, D is no larger than 1, and from Equation (71), p is slightly smaller than r.

On the other hand, Figure 6.14 presents that volume fraction affects damage revolution greatly. Still with the slight difference

between p and r, damage and plastic strain will increase largely if volume fraction increases.

From Figure 6.15, we find volume fraction of inclusion not only effects the elastic range, but also plastic part. We have known that the slope of linear elastic curve shows effective performance of composites, also, the rate of stress increment increases with the increasing of volume fraction.

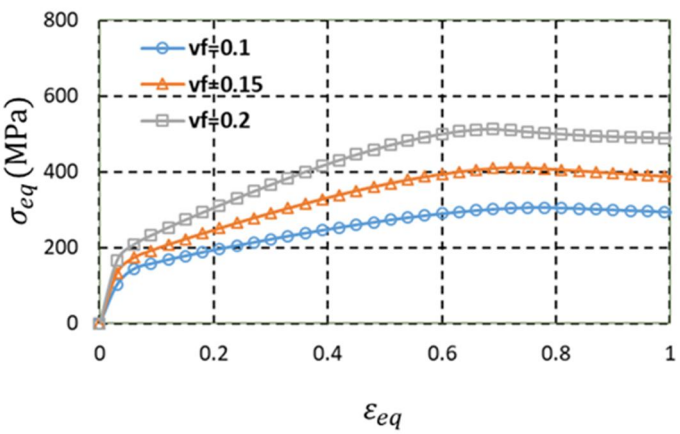

Figure 6.15 The effect of volume fraction

(Interfacial damage: α=0.3, β=0; Aspect Ratio: 0.01)

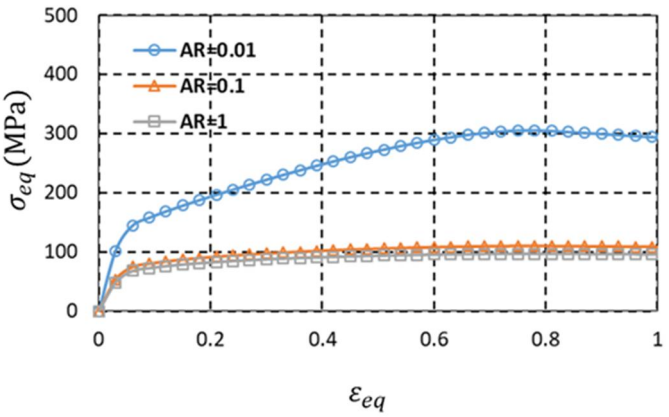

Figure 6.16 The effect of volume fraction

(Interfacial damage: α=0.3, β=0; Volume fraction: 0.1)

Aspect ratio, as another factor which influences the stress–strain curve greatly. In the Figure 6.16, when aspect ratio increases, which means the shape of inclusion changes from a disk like plate to a sphere, effective properties reduces. We also find, from sphere shape inclusion to cylinder shape fiber, in another word, AR=∞, the effective properties will still decrease.

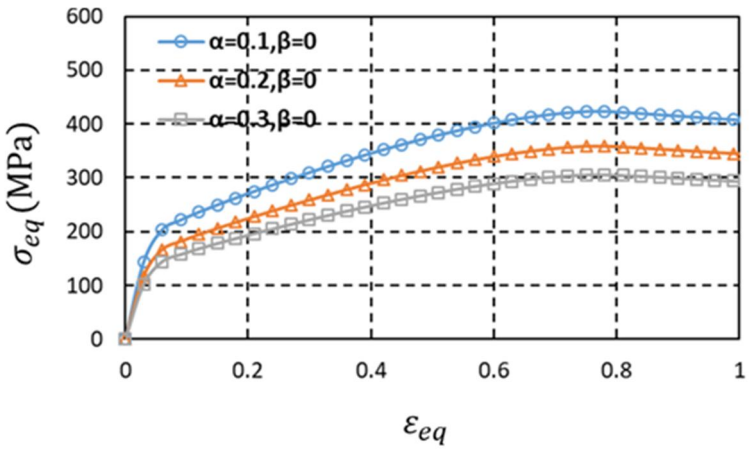

Figure 6.17 The effect of tangential damage

(Aspect Ratio: 0.01; Volume fraction: 0.1)

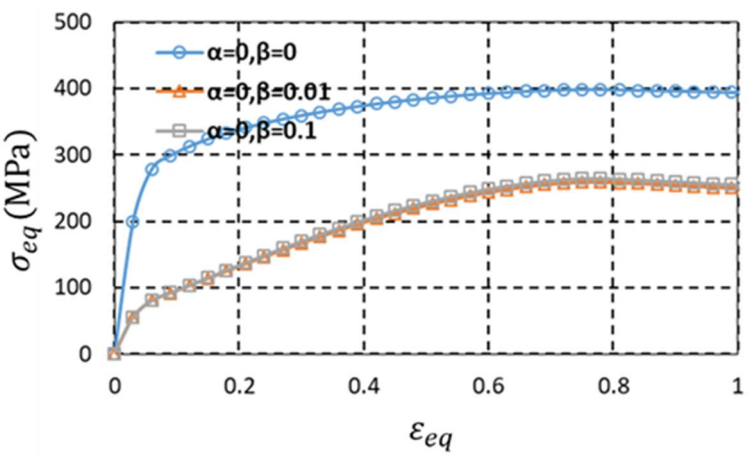

Figure 6.18 The effect of normal damage

(Aspect ratio: 0.01; Volume fraction: 0.1)

In Figure 6.17 and Figure 6.18, it mainly indicates how interfacial damage affect stress−strain curve. α, which means tangential damage have softer effect comparing with radial damage β. Curves in various tangential damage α shows similar tendency both in elastic part and plastic range, while β influences elastic range greatly.

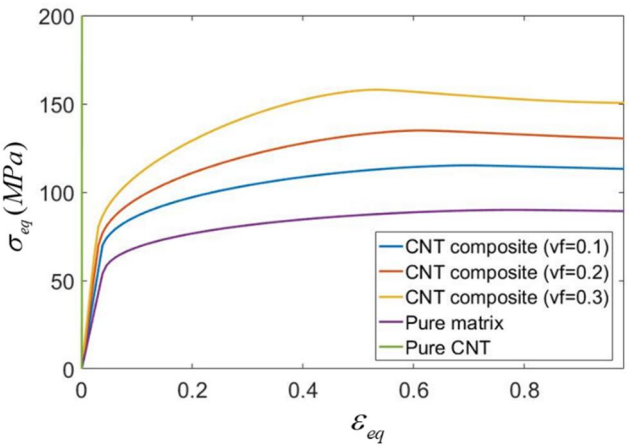

Figure 6.19 CNT nanocomposites elasto-plastic simulation

(waviness: 0, α=0.3, β=0)

Figure 6.19 shows the plastic performance of CNT nanocomposites, to achieve cylinder shape CNT fiber model, we set aspect ratio to be very large which is close to infinite. And we compare the performance among pure CNT fiber, pure matrix and CNT nanocomposites with various volume fraction. The CNT fiber

has significant mechanical properties which increase greatly. And CNT nanocomposites show better effective properties both in elastic and plastic range. Although every 10% of CNT inclusion will greatly improve the properties.

7. Conclusion and future works

7.1. Conclusion

In this thesis, we first develop a spatial random field for further stochastic simulation and then a linear CNT nanocomposites model is presented with Mori−Tanaka homogenization method in elastic range. Not only doing simulation on influence of CNT fiber shape in nanocomposites, but orientation is also mentioned. In addition, we provide a nonlinear multiscale damage model of nanocomposites which is based on Lemaitre−Chaboche model to do research on plastic properties of composites. So combining with spatial randomness, linear and nonlinear Mori−Tanaka models, we have a completed model to simulate CNT composites' shapes orientations and elastic, plastic properties.

In linear micromechanics model simulation, we present the effects on volume fraction, waviness, interfacial damage and correlation length with stochastic random fields. Increasing volume fraction have a positive influence while waviness and interfacial

damage have negative influence on main direction of CNT nanocomposites. The effect of correlation length, a variable related to random fields, is conspicuous since it changes the stochastic radius around a random field point.

Then, in nonlinear mechanical damage model, a two-phase composites model with interfacial and ductile damage is developed. We present the evolution of plastic strain and ductile damage. And we discuss the influence of volume fraction, interfacial damage and aspect ratio. The effects of volume fraction and interfacial damage are similar with the effects on linear elastic CNT nanocomposites model. The effect of aspect ratio shows the disk like inclusion with small aspect ratio will have better effective properties than fiber like inclusion with large aspect ratio. At last, results of a CNT composites model is presented with various volume fraction to show nonlinear damage evolution.

7.2. Future works

In this thesis, we simulate the effects of material properties including waviness, volume fraction, orientation and damage on CNT nanocomposites. Also, combining with the performance of elasto-plastic properties, CNT nanocomposites model have been well-simulated.

With the completed CNT nanocomposites model, we can do further effort to make model more realistic. Fist we can introduce waviness in nonlinear interfacial damage model and then, develop random fields with 3D KLE we introduced in the thesis to do stochastic simulation. For instance, stochastic aspect ratio shapes and orientation in nonlinear micromechanics model. Also, instead of regular sinuous wavy shape and perfect matrix base, CNT fiber is more complicated in matrix. Modeling well-matched fiber appearance and ductile damage model can improve the exist simulation.

Also, based on elasto-plastic simulation of CNT nanocomposites, elasto-viscoplastic can also been well-researched. Elasto-viscoplastic composites provide great mechanical performance which

can be applied in electronic fields. The extend research on elasto-viscoplastic composites can substitute the original elasto-plastic revolution and combine with viscoplastic mechanism.

8. Reference

[1] Collins, P. G., and Avouris, P., 2000, "Nanotubes for electronics," Sci Am, 283(6), pp. 62-+.

[2] Iijima, S., 1991, "Helical Microtubules of Graphitic Carbon," Nature, 354(6348), pp. 56-58.

[3] Mittal, G., Dhand, V., Rhee, K. Y., Park, S. J., and Lee, W. R., 2015, "A review on carbon nanotubes and graphene as fillers in reinforced polymer nanocomposites," J Ind Eng Chem, 21, pp. 11-25.

[4] Liew, K. M., Lei, Z. X., and Zhang, L. W., 2015, "Mechanical analysis of functionally graded carbon nanotube reinforced composites: A review," Composite Structures, 120, pp. 90-97.

[5] Gohardani, O., Elola, M. C. A., and Elizetxea, C., 2014, "Potential and prospective implementation of carbon nanotubes on next generation aircraft and space vehicles: A review of current and expected applications in aerospace sciences," Prog Aerosp Sci, 70, pp. 42-68.

[6] Rafiee, R., and Moghadam, R. M., 2014, "On the modeling of carbon nanotubes: A critical review," Composites Part B-Engineering, 56, pp. 435-449.

[7] De Volder, M. F. L., Tawfick, S. H., Baughman, R. H., and Hart, A. J., 2013, "Carbon Nanotubes: Present and Future Commercial Applications," Science, 339(6119), pp. 535-539.

[8] Khan, S. U., Pothnis, J. R., and Kim, J. K., 2013, "Effects of carbon nanotube alignment on electrical and mechanical properties of epoxy

nanocomposites," Composites Part a-Applied Science and Manufacturing, 49, pp. 26-34.

[9] Zare, Y., and Garmabi, H., 2014, "Attempts to Simulate the Modulus of Polymer/Carbon Nanotube Nanocomposites and Future Trends," Polym Rev, 54(3), pp. 377-400.

[10] Shokrieh, M. M., and Rafiee, R., 2010, "A review of the mechanical properties of isolated carbon nanotubes and carbon nanotube composites," Mech Compos Mater, 46(2), pp. 155-172.

[11] Hammerand, D. C., Seidel, G. D., and Lagoudas, D. C., 2007, "Computational micromechanics of clustering and interphase effects in carbon nanotube composites," Mechanics of Advanced Materials and Structures, 14(4), pp. 277-294.

[12] Fisher, F. T., Bradshaw, R. D., and Brinson, L. C., 2002, "Effects of nanotube waviness on the modulus of nanotube-reinforced polymers," Applied Physics Letters, 80(24), pp. 4647-4649.

[13] Bradshaw, R. D., Fisher, F. T., and Brinson, L. C., 2003, "Fiber waviness in nanotube-reinforced polymer composites-II: modeling via numerical approximation of the dilute strain concentration tensor," Composites Science and Technology, 63(11), pp. 1705-1722.

[14] Shao, L. H., Luo, R. Y., Bai, S. L., and Wang, J., 2009, "Prediction of effective moduli of carbon nanotube-reinforced composites with waviness and debonding," Composite Structures, 87(3), pp. 274-281.

[15] Anumandla, V., and Gibson, R. F., 2006, "A comprehensive closed form micromechanics model for estimating the elastic modulus of nanotube-

reinforced composites," Composites Part a-Applied Science and Manufacturing, 37(12), pp. 2178-2185.

[16] Seidel, G. D., and Lagoudas, D. C., 2006, "Micromechanical analysis of the effective elastic properties of carbon nanotube reinforced composites," Mechanics of Materials, 38(8-10), pp. 884-907.

[17] Odegard, G. M., Gates, T. S., Wise, K. E., Park, C., and Siochi, E. J., 2003, "Constitutive modeling of nanotube-reinforced polymer composites," Composites Science and Technology, 63(11), pp. 1671-1687.

[18] Yang, B. J., Jang, J. U., Eem, S. H., and Kim, S. Y., 2017, "A probabilistic micromechanical modeling for electrical properties of nanocomposites with multi-walled carbon nanotube morphology," Composites Part a-Applied Science and Manufacturing, 92, pp. 108-117.

[19] Subramanian, N., Rai, A., and Chattopadhyay, A., 2015, "Atomistically informed stochastic multiscale model to predict the behavior of carbon nanotube-enhanced nanocomposites," Carbon, 94, pp. 661-672.

[20] Chamis, C. C., 1984, "Simplified Composite Micromechanics Equations for Hygral, Thermal, and Mechanical-Properties," Sampe Quart, 15(3), pp. 14-23.

[21] C. T. Sun,1996, “Prediction of Composite Properties from Representative Volume Element“, Compo. Sci & Technology 56. 171-179.

[22] Z. H. Xia, 2003, “A unified periodical boundary conditions for representative volume elements of composites and applications“, International Journal of Solids and Structures 40. 1907-1921.

[23] C. Chamis, "Mechanics of Composite Materials: Past, Present, and Future," Journal of Composites, Technology and Research 11, no. 1 (1989): 3-14. https://doi.org/10.1520/CTR10143J.

[24] Mofid Mahdi, 2001, “A finite element model for the orthogonal cutting of fiber-reinforced composite materials“, Materials Processing Technology 113. 373-377.

[25] A. V. Desai, 2005, “Mechanics of the interface for carbon nanotube-polymer composites”, Thin-Walled Structures 43. 1787-1803.

[26] J. C. Halpin, 1976, “The Halpin-Tsain Equations: A Review”, Polymer Engineering and Science, 344-352.

[27] Coleman JN, Khan U, Blau WJ, Gun’ko YK, 2006, “Small but Strong: a review of the mechanical properties of carbon nanotube polymer composites”, Carbon 44. 1624-52.

[28] Erik T Thostenson, Tsu-wei Chou, 2003, “On the elastic properties of carbon nanotube-based composites: modeling and characterization”, Physics D: Applied Physics 35-5.

[29] D. Hopkins and C. Chamis, "A Unique Set of Micromechanics Equations for High-Temperature Metal Matrix Composites," in Testing Technology of Metal Matrix Composites, ed. N. Adsit and P. DiGiovanni (West Conshohocken, PA: ASTM International, 1988), 159-175. https://doi.org/10.1520/STP25950S.

[30] A. R. Bunsell, J Renard, 2005, “Fundamentals of a fibre Reinforced Composite Materials”.

[31] Benny BR, 2012, “Effective moduli of multi-scale composites”, Compo. Sci & Technology 72. 566-573.

[32] Caruso and C. Chamis, "Assessment of Simplified Composite Micromechanics Using Three-Dimensional Finite-Element Analysis," Journal of Composites, Technology and Research 8, no. 3 (1986): 77-83. https://doi.org/10.1520/CTR10326J.

[33] Finegan IC. Analytical and experimental study of improvement of damping at the micromechanical level in polymer composite materials by the use of special fiber coatings. PhD. D. Dissertation. Detroit(MI): Wayne State University, 1997.

[34] Jun Huang. 2013. "Equivalent continuum models of carbon nanotube reinforced polypropylene composites". Materials and Design 50. 936-945.

[35] MM Shokrieh, 2010, "Stochastic multi-scale modeling of CNT/polymer composites", Computational Materials Science 50, 437-446.

[36] HM Duong, 2008, "Computational modeling of the thermal conductivity of single-walled carbon nanotube–polymer composites", Nanotechnology 19 065702.

[37] Mori, T. and K. Tanaka, Average Stress in Matrix and Average Elastic Energy of Materials with Misfitting Inclusions. Acta Metallurgica, 1973. 21(5): p. 571-574.

[38] Qiu, Y.P. and G.J. Weng, On the Application of Mori Tanaka Theory Involving Transversely Isotropic Spheroidal Inclusions. International Journal of Engineering Science, 1990. 28(11): p. 1121-1137.

[39] Qu, J. and M. Cherkaoui, Fundamentals of Micromechanics of Solids. 2006, New Jersey: Wiley.

[40] Pettermann, H.E., et al., A thermo-elasto-plastic constitutive law for inhomogeneous materials based on an incremental Mori-Tanaka approach. Computers & Structures, 1999. 71(2): p. 197-214.

[41] Pettermann, H.E., et al., An Incremental Mori-Tanaka Homogenization Scheme for Finite Strain Thermoelasto-plasticity of MMCs. Materials, 2010. 3(1): p. 434-451.

[42] Koyama, S., et al., A modification of the Mori-Tanaka estimate of average elastoplastic behavior of composites and polycrystals with interfacial debonding. Mechanics of Materials, 2011. 43(10): p. 538-555.

[43] Czarnota, C., et al., Modeling of the cyclic behavior of elastic-viscoplastic composites by the additive tangent Mori-Tanaka approach and validation by finite element calculations. International Journal of Solids and Structures, 2015. 56-57: p. 96-117.

[44] Sadowski, P., K. Kowalczyk-Gajewska, and S. Stupkiewicz, Response discontinuities in the solution of the incremental Mori-Tanaka scheme for elasto-plastic composites. Archives of Mechanics, 2017. 69(1): p. 3-27.

[45] Sadowski, P., K. Kowalczyk-Gajewska, and S. Stupkiewicz, Consistent treatment and automation of the incremental Mori-Tanaka scheme for elasto-plastic composites. Computational Mechanics, 2017. 60(3): p. 493-511.

[46] Tan, H., et al., The Mori-Tanaka method for composite materials with nonlinear interface debonding. International Journal of Plasticity, 2005. 21(10): p. 1890-1918.

[47] Tan, H., et al., Constitutive behaviors of composites with interface debonding: the extended Mori-Tanaka method for uniaxial tension. International Journal of Fracture, 2007. 146(3): p. 139-148.

[48] Mercier, S. and A. Molinari, Homogenization of elastic-viscoplastic heterogeneous materials: Self-consistent and Mori-Tanaka schemes. International Journal of Plasticity, 2009. 25(6): p. 1024-1048.

[49] Peng, X.H., et al., Extension of Combined Self-Consistent and Mori-Tanaka Approach to Evaluation of Elastoplastic Property of Particulate Composites. Acta Mechanica Solida Sinica, 2013. 26(1): p. 71-82.

[50] Bohm, H.J. and S. Nogales, Mori-Tanaka models for the thermal conductivity of composites with interfacial resistance and particle size distributions. Composites Science and Technology, 2008. 68(5): p. 1181-1187.

[51] Vorel, J. and M. Sejnoha, Evaluation of homogenized thermal conductivities of imperfect carbon-carbon textile composites using the Mori-Tanaka method. Structural Engineering and Mechanics, 2009. 33(4): p. 429-446.

[52] Kamarian, S., M. Shakeri, and M.H. Yas, Natural Frequency Analysis and Optimal Design of CNT/Fiber/Polymer Hybrid Composites Plates Using Mori-Tanaka Approach, GDQ Technique, and Firefly Algorithm. Polymer Composites, 2018. 39(5): p. 1433-1446.

[53] Garcia-Macias, E., et al., Eshelby-Mori-Tanaka approach for post-buckling analysis of axially compressed functionally graded CNT/polymer composite cylindrical panels. Composites Part B-Engineering, 2017. 128: p. 208-224.

[54] Heshmati, M. and M.H. Yas, Free vibration analysis of functionally graded CNT-reinforced nanocomposite beam using Eshelby-Mori-Tanaka approach. Journal of Mechanical Science and Technology, 2013. 27(11): p. 3403-3408.

[55] Xin, L.B., et al., An approximate analytical solution based on the Mori-Tanaka method for functionally graded thick-walled tube subjected to internal pressure. Composite Structures, 2016. 135: p. 74-82.

[56] Shen, H.S. and Z.X. Wang, Assessment of Voigt and Mori-Tanaka models for vibration analysis of functionally graded plates. Composite Structures, 2012. 94(7): p. 2197-2208.

[57] Imani, S.M., et al., The modified Mori-Tanaka scheme for the prediction of the effective elastic properties of highly porous ceramics. Ceramics International, 2018. 44(14): p. 16489-16497.

[58] Qu, J.M., The Effect of Slightly Weakened Interfaces on the Overall Elastic Properties of Composite-Materials. Mechanics of Materials, 1993. 14(4): p. 269-281.

[59] Barai, P. and G.J. Weng, A theory of plasticity for carbon nanotube reinforced composites. International Journal of Plasticity, 2011. 27(4): p. 539-559.

[60] Pan, Y., et al., Interface effects on the viscoelastic characteristics of carbon nanotube polymer matrix composites. Mechanics of Materials, 2013. 58: p. 1-11.

[61] Shokrieh, M.M., R. Ghajar, and A.R. Shajari, The effect of time-dependent slightly weakened interface on the viscoelastic properties of

CNT/polymer nanocomposites. Composite Structures, 2016. 146: p. 122-131.

[62] Yang, S., et al., Nonlinear multiscale modeling approach to characterize elastoplastic behavior of CNT/polymer nanocomposites considering the interphase and interfacial imperfection. International Journal of Plasticity, 2013. 41: p. 124-146.

[63] Lee, S. and S.H. Ryu, Theoretical study of the effective modulus of a composite considering the orientation distribution of the fillers and the interfacial damage. European Journal of Mechanics - A/Solids, 2018. 72: p. 79-87.

[64] Tsai, C.H., et al., The effect of inclusion waviness and waviness distribution on elastic properties of fiber-reinforced composites. Composites Part B-Engineering, 2011. 42(1): p. 62-70.

[65] Shang, S., and Yun, G. J., 2013, "Stochastic Finite Element with Material Uncertainties: Implementation in a General-Purpose Simulation Program," Finite Elements in Analysis and Design, 64, pp. 65-78.

[66] Mura, T., Micromechanics of Defects in Solids. 2nd Revised Edition ed. 1987, Dordrecht: Kluwer Academic Publishers.

[67] Qu, J.M., Eshelby Tensor for an Elastic Inclusion with Slightly Weakened Interface. Journal of Applied Mechanics-Transactions of the Asme, 1993. 60(4): p. 1048-1050.

[68] Weng, G.J., Some Elastic Properties of Reinforced Solids, with Special Reference to Isotropic Ones Containing Spherical Inclusions. International Journal of Engineering Science, 1984. 22(7): p. 845-856.

[69] Yanase, K., S. Moriyama, and J.W. Ju, Effects of CNT waviness on the effective elastic responses of CNT-reinforced polymer composites. Acta Mechanica, 2013. 224(7): p. 1351-1364.

[70] Hsiao, H.M. and I.M. Daniel, Elastic properties of composites with fiber waviness. Composites Part a-Applied Science and Manufacturing, 1996. 27(10): p. 931-941.

[71] Sharma, A., Nehra, S. P., Vijay, Y. K., and Jain, I. P., 2016, "Fast mass and charge transport through electrically aligned CNT/polymer nanocomposite membranes," Int J Energ Res, 40(6), pp. 770-775.

[72] Huang, J.H., Some closed-form solutions for effective moduli of composites containing randomly oriented short fibers. Materials Science and Engineering a-Structural Materials Properties Microstructure and Processing, 2001. 315(1-2): p. 11-20.

[73] W. L. Azoti, 2013, “Mean-field constitutive modeling of elasto-plastic composites using two (2) incremental formulations”,Composites Structures 105, 256-262.

[74] P. H. Dederichs, R. Zeller, Variational treatment of the elastic constants of disordered materials, Zeitschrift fur Physik A hadrons Nucl Volume 259, Number 2, 103-116, DOI: 10.1007/BF01392841.

[75] Vieville P, Bonnet AS, Lipinski P. Modelling effective properties of composite materials using the inclusion concept. General consideration. Arch Mesh 2006; 58(3):207-39.

[76] Andrews, R., et al., Fabrication of carbon multiwall nanotube/polymer composites by shear mixing. Macromolecular Materials and Engineering, 2002. 287(6): p. 395-403.

[77] Guru, K., et al., Effect of Interface on the Elastic Modulus of CNT Nanocomposites. Journal of Nanomechanics and Micromechanics, 2016. 6(3).

[78] S. Oller, 1990, “Finite Element Nonlinear Analysis of Concrete Structures Using a ‘Plastic Damage Model.’ ”, Engineering Fracture Mechanics Vol. 35, 219-231

[79] C. T. Sun, J. L. Chen, 1989, “A Simple Flow Rule for Characterizing Nonlinear Behavior of Fiber Composites”, Journal of Composite Material, Vol. 23

[80] S. Kyriakides, 1995, “On the Compressive Failure of Fiber Reinforced Composites”, Solids Structures Vol. 32, 689-738

[81] R. A. Schapery, 1997, “Nonlinear Viscoelastic and Viscoplastic Constitutive Equations Based on Thermodynamics”, Mechanics of Time-Dependent Materials 1: 209-240

[82] Amir Mirmiran, 2000, “Nonlinear finite element modeling of concrete confined by fiber composites”, Finite Elements in Analysis and Design 35, 79-96

[83] Ehsan Mohammadpour, 2014, “Modeling the tensile stress-strain response of carbon nanotube/ polypropylene nanocomposites using nonlinear representative volume element”, Materials and Design 58, 36-42

국문초록

확률적 카본나노튜브 나노복합재료를 위한 선형 & 비선형 미소역학 모델

주 비 연

기계항공공학부

서울대학교 대학원

탄소나노튜브(CNT)는 기계적, 전기적, 화학적 특성이 뛰어나기 구조 재료, 스텔스 재료, 센서, 콘덴서, 전기 장치 등 다양한 용도에 나노필러로 연구되어 왔다. CNT 나노복합재료에 대한 연구는 특히 합성기술과 제조기술 분야에 많은 진전이 있어왔음에도 불구하고 복잡한 특성, 비균일적 분산과 복잡한 다중물리적 특성으로 인해 설계, 모델링 및 분석은 상대적으로 덜 성숙되어 있다. 더욱이, 나노 싸이즈 CNT 필러의 고정밀 모델링을 통한 매크로 실험스케일 에서의 물리적 거동을 예측하기 위해서는 본질적으로 멀티스케일 접근법을 필요로 하며 나노스케일에서 매크로스케일로의 브리징을 위해서는 미소역학이론과 균질화가 매우 핵심적인 기술이다.

본 논문에서는 CNT 나노복합재료를 위한 비선형 미소역학 모델에 대한 새로운 접근법을 제시함으로써 일반 나노복합재료의 추계적 멀티스케일 모델링 및 분석을 위한 프레임워크를 개발하는 것으로 한다. 3 차원 공간에서 나노 싸이즈 필러의 일반적 설계 변수의 확률적 변화를 고려할 수 있는 추계학적 모델링 프레임워크가 제안되었다. 예로 추계학적 모델링 기법을 나노 필러의 통계적 배향 모델링에 적용하였다. 그 뒤 균질화법으로 널리 사용되는 Mori-Tanaka 미소역학모델을 적용하여 폴리머 매트릭스의 연성 손상 소성 및 매트릭스와 CNT 나노 필러 간의 계면손상은 증분-반복적인 Mori-Tanaka 미소역학이론을 기반으로 한 프레임워크 내에서 모델링하였다. 계면손상을 시뮬레이션 하기 위해 선형 스프링 모델을 Mori-Tanaka 방식과 결합하여 CNT 섬유 방향이 나노복합 재료의 유효강성에 미치는 영향을 연구하였다. J2 유동 법칙과 Lemaitre-Chaboche 손상 모델링 방법을 통해 소성변형 특성을 예측하였다. 수치해석에서는 체적분율, 형상비, 계면 손상 및 연성 손상을 고려하였다. 탄소성 특성은 연성과 계면손상, 기타 복합 재료 특성에 의해 크게 영향을 받는 것으로 나타났다.

Keywords: 확률적 시뮬레이션, 연성인 손상, 모리타나카, 계면의 손상, CNT 합성재료

Student Number: 2017-21362